TD-01-062
10/01

Fermi National Accelerator Laboratory
Technical Division / Development & Test Dept.
PO Box 500 MS 316
Batavia, IL 60510
FAX : 630-840-2383

ACCELERATOR PHYSICS AND TECHNOLOGY LIMITATIONS IN STAGE II TYPE VERY LARGE HADRON COLLIDERS

Summary of contributions to the M4 WG at the Snowmass 2001 conference

P. Bauer, P. Limon, M. Dietrich, S. Peggs*, M. Syphers, N. Solyak

Abstract:

One of the charges of the Snowmass conference organizing committee was to investigate the major technology limitations to ultimate energy and luminosity in very large hadron colliders. The following is an attempt at answering this question. First, the main accelerator physics limitations to ultimate energy and luminosity in future energy frontier hadron colliders were identified. They are synchrotron radiation power, proton-collision debris power in the IR, number of events per crossing, stored energy per beam and beam-stability. Quantitative estimations of these limiting parameters were made and justified. The limitations were inscribed into the particle energy versus machine size plane to delimit the boundaries for possible accelerators. Finally, accelerator simulations were performed in order to estimate the maximum achievable luminosities, given the specified set of limitations. Results and conclusions are presented.

*CAD Accelerator Physics, Brookhaven National Laboratory, Upton, NY 11973

TABLE OF CONTENT

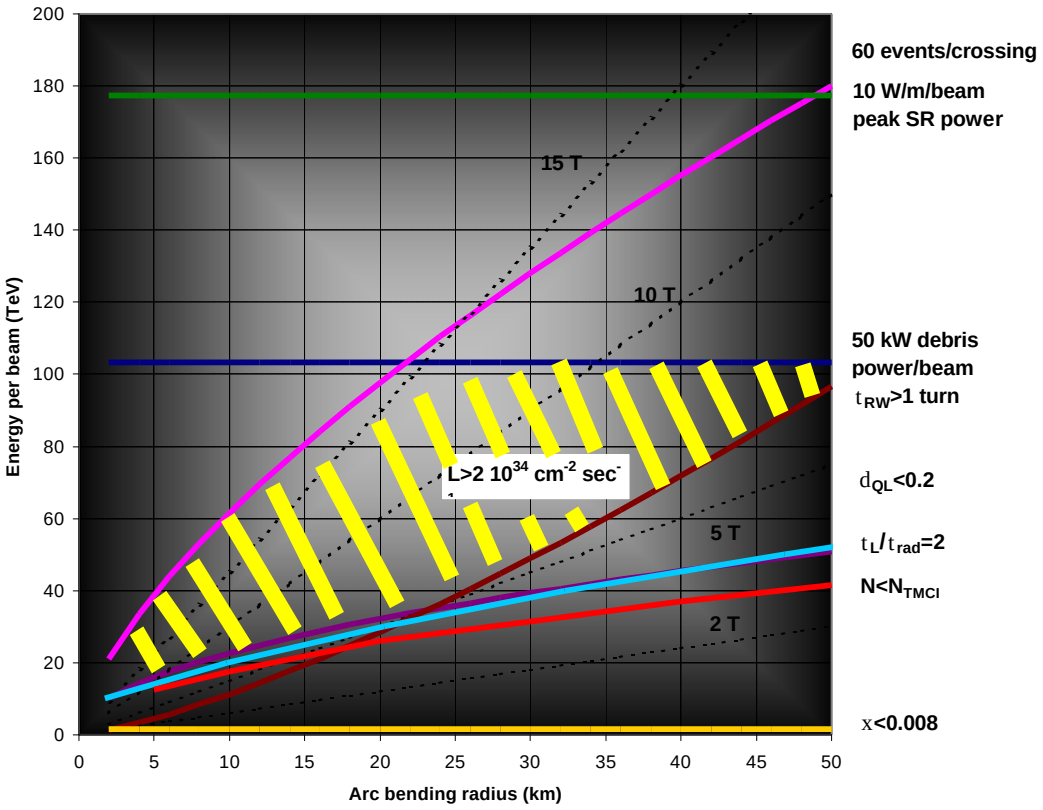
Energy per beam (TeV)
Arc bending radius (km)
15 T
10 T
5 T
2 T
L>2 10^34 cm^-2 sec^-1
60 events/crossing
10 W/m/beam
peak SR power
50 kW debris
power/beam
t_RW>1 turn
d_QL<0.2
t_L/t_rad=2
N<N_TMCI
x<0.008

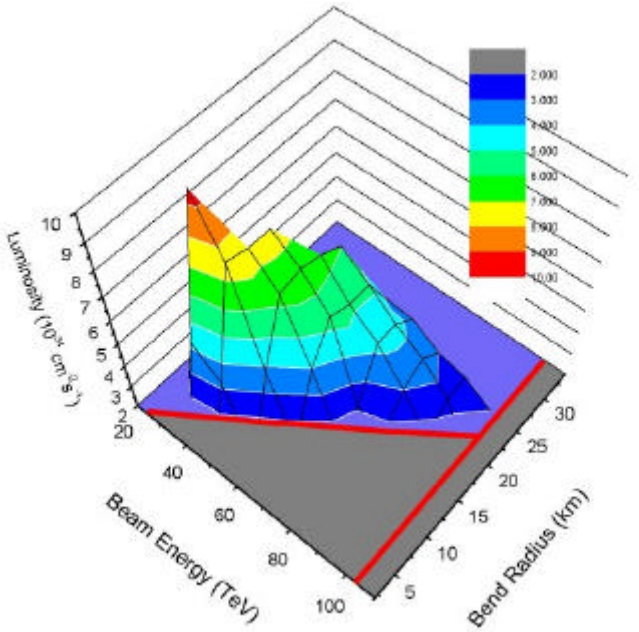
Luminosity (10^x cm^-2 s^-1)
Beam Energy (TeV)
Bend Radius (km)

1.0 INTRODUCTION

The following items have been identified as the main accelerator physics limitations to ultimate energy and luminosity in future energy frontier hadron colliders:

- synchrotron radiation power
- proton-collision debris power in the IR
- number of events per crossing
- stored energy per beam
- beam stability

Some of the items in this list are discussed in more detail in other sub-group reports of the Snowmass conference. See for example the discussion of the beam-screen and the photon-stop systems used to cope with synchrotron radiation in the WG-T2-Magnets report or in a special note [1]. Or the discussions of magnet and detector technology and the IR debris power issues, in the T2, E4, T1 WG summary reports. More details on issues pertaining to beam-stability can be found in the recent BNL/FNAL VLHC accelerator physics report [2] and the Snowmass collective effects working group results. This discussion aims at determining the accelerator performance limitations, namely in center of mass energy and luminosity, related to each of the items listed above and to map out the regions of accelerator physics parameter space accessible to the next generation of energy frontier hadron colliders. The currently proposed VLHC, which will be often referred to in the following is best described in [3].

2.0 QUANTIFICATION OF THE LIMITS

2.1 Synchrotron Radiation Power

What is the synchrotron radiation (SR) power limitation in hadron colliders? Cern's LEP, which is currently considered as the last circular electron machine, produced ~400 W/m/beam of synchrotron radiation power. Therefore it can be assumed that the order of magnitude of 100 W/m/beam of synchrotron radiation power is a hard limit as well for proton machines. One has to be careful though, because the technology needed to handle such a large synchrotron radiation power has not been developed in the field of hadron colliders yet. Especially complicating is the fact that all high field hadron colliders use superconducting magnets. The cryogenic environment strongly complicates and raises the cost of the removal of the power deposited by synchrotron radiation. On the other hand, the extensive experience with synchrotron radiation absorbers in lepton machines and light sources, should make us confident that we can manage to extract a synchrotron radiation power load of 100 W/m/beam from a cryogenic magnet system in a proton-beam environment at minimized cost with so called photon-stopers. Fermilab and Argonne National lab are currently involved in R&D aiming at testing such a photon-stop. However, as long as photon-stops are not acquired technology and to account for accelerator scenarios in which photon stops cannot be used, it is more reasonable to limit the synchrotron radiation power to a level that can be handled as well with the more traditional beam screen solution. Preliminary calculations, done in the context of the recent VLHC feasibility study [3] indicate that 10 W/m/beam peak radiation power can be handled by a beam screen installed in a ~40 mm magnet aperture (see as well [4]), leaving an stay clear beam area with 20 mm ∅.

2.2 IR Debris Power

The debris emanating from the beam interaction regions (IR) affects detector operation, results in power deposition in the interaction-region (IR) magnets and is ultimately the cause of radio-activation in the detector vicinity. The LHC accelerator at CERN is projected to produce ~ 1 kW of debris power per IR. The currently proposed VLHC [3], in its first stage, would produce 2·3 kW of debris power per IR, which can be absorbed by a succession of shields much like in the LHC. The current proposal for the VLHC in its second stage, however, foresees a debris power level of up to 50 kW per beam. A detailed analysis of possible shielding scenarios has not been made yet. Preliminary analysis predicts the need of absorbers in the bores of the interaction region magnets together with a series of collimation shields at the end of the detector and interspersed between the IR magnets to cope with the neutral debris (~30%). In the calculations presented here a 50 kW per beam debris power was set as a limit. It is hoped that this benchmark will be achieved in the course of continued IR design activity.

2.3 Events per Crossing

It is the usual approach to design an accelerator for the maximum rate of events per bunch crossing. Again, going from a few events per bunch crossing in the LHC to 19 in the VLHC-stage 1 [3] and 60 in the VLHC-stage 2 [3] is not accomplished in detector design yet. A limit of 60 events per crossing was chosen as the feasibility limit here. An important parameter in this context is the bunch spacing time. The time resolution of the detector has to be small enough to accommodate a bunch spacing of ~19 ns in the VLHC-2 design. This seems feasible with current technology and therefore a bunch spacing of 12 ns was chosen here, based on the assumption that future detector technology will be up to this level.

2.4 Beam Stored Energy

The VLHC-2 [3] in its ultimate 200 TeV stage has a beam stored energy of 4.3 GJ. Such a high level of beam energy is yet unknown. Almost arbitrarily, the limiting beam stored energy level was specified to 10 GJ in this study.

2.5 Beam Stability

The small aperture of the VLHC-1 beam tube, coupled with its room-temperature resistivity may induce beam instabilities. The aperture chosen, 18 mm x 28 mm is on the verge of being too small, and will require significant R&D and beam studies to guarantee good operation. Nevertheless, in principle, all of the instabilities have solutions at hand.
The dominant beam instabilities in the VLHC are of the transverse type. They depend strongly on the magnet aperture. All of the instabilities depend on the beam current in some way; so improved emittance (and therefore fewer protons needed to reach the desired luminosity) would improve the situation. In the currently proposed VLHC [3], the most important instabilities are the Laslett tune shift, the resistive wall instability, and the fast head-tail, or transverse-mode coupling instability (TMCI).

2.5.1 Beam-Beam Tune-shift

The beam-beam tune-shift is related to the transverse space charge forces, occurring during the interpenetration of colliding bunches in and around the IP's. The non-linearity

of these forces causes a tune-spread within the bunches, which is the more dangerous aspect of this effect. The tune-spread correlates with the overall tune-shift and therefore it is the tune-shift limit that is specified. It scales linearly with the bunch-population and is inversely proportional to the emittance. Beam-beam tune-shift is the cause why in synchrotron radiation damped machines the damping usually cannot be allowed to proceed to completion. The limiting tune-shift rises as a function of damping decrement, thus less damping and a smaller ring size help. Flat beams produce ~ 50% less beam-beam tune-shift than comparable round beams. Experimental and simulation data indicate a maximum allowable beam-beam tune-shift of 0.008 at a damping decrement of $\sim 10^{-7}$, which is the condition in the currently proposed stage 2 VLHC [3]. The calculations presented here assume the same maximum allowable beam-beam tune-shift.

2.5.2 Resistive Wall Instability

The resistive wall instability is induced by the low frequency (of the order of the revolution frequency) transverse impedance seen by the beam. It depends linearly on the average beam current. The resistive wall instability appears as a growth of the betatron amplitude of the beam. The low frequency transverse impedance, which is strongly dominated by the resistive wall of the beam tube, is proportional to the magnet aperture b, the thickness of the high conductivity coating on the inside of the beam-tube and inversely proportional to the machine size. To reduce the impedance the magnet aperture has to be increased together with the coating thickness, while the machine size is to be reduced. The beam oscillations can be controlled and/or corrected if there is enough time. Therefore the e-folding time of the resistive wall instability has to be at least of the order of one turn. The currently proposed stage 1 VLHC [3] has a resistive wall instability e-folding time of less than one turn. Feedback systems and related kickers distributed around the ring will be required to counteract the transverse kicks induced by the low frequency transverse wake. In this study, however, a maximum e-folding time of 1 turn was assumed to be the design limit. This approach assumes a priori the use of feedback systems or other related corrective measures.

2.5.3 Fast Head Tail Instability (TMCI)

The fast head-tail instability (or TMCI) is related to the high-frequency (of the order of the bunch-length frequency c/l_b) part of the impedance spectrum. The instability appears as a resonant wiggling of the bunches, excited by transverse kicks induced by the wake-fields caused by the protons at the head of the bunch. It scales linearly with the bunch current. Similarly to the low frequency case discussed before, the high frequency impedance is proportional to aperture and ring size, and the coating thickness is appropriately replaced by the skin-depth. Distinctively from the low frequency impedance it is not the resistive wall that dominates, but rather the sum of the contributions of smaller size components such as bellows, BPM's, beam-screen pumping slots and photon-stops. In this study we assumed the limitation to occur when the bunch intensity reaches the TMCI bunch current threshold. This approach assumes additional measures, such as coalescing schemes, RF quadrupoles,..etc, to gain operational margin.

2.5.4 Laslett Tune-Shift

The Laslett tune-shift (or spread) is the result of defocusing forces on the protons inferred by the space charge, the mirror charges on the (conducting) beam tube wall and the magnetic boundary conditions in the magnet pole faces induced by the bunch current. Coherent tune-shifts are benign, because they can easily be corrected by changing the tune of the machine. As explained above in the case of the beam-beam tune-shift, it is the tune-spread, which is proportional to the overall tune-shift, that has to be limited. In ultra-relativistic beams the space charge effects are negligible. The main contributions to the effect come from the (dc) mirror charges in the beam-tube wall. Therefore the Laslett tune shift scales with the bunch current (and thus the luminosity) and the square of the magnet aperture. Partial filling of the ring during injection can induce a Laslett tune spread along the bunch train. These bunch-to-bunch tune variations, typically of the order of 10 %, can be alleviated by injecting the beam in a symmetric manner, i.e. with bunches entering far apart from each other and gradually filling in between the already injected bunches. We assumed a maximum coherent Laslett tune-shift of 0.2 in this study.

2.6 Energy and Luminosity

The most interesting question related to the design of the next large hadron collider is that of the optimal machine size for a given ultimate particle energy. The most important parameter in this context is of course the cost, which will not be discussed here. Secondarily it would be interesting, and that is what this study is attempting to do, to map out the possible combinations of ring-size and particle energy, that are accessible to the machine designers, given the technological limitations described above. In addition it is important to know the maximum luminosities that can be achieved in each energy/ring-size combination. In order to do that it is necessary to simulate the accelerator operation for all energy/bending radius combinations. This is a tremendous task. Therefore, this study proceeded differently: First, the areas in the energy/size space excluded by each of the above mentioned constraints were calculated. To do this, each of the constraining magnitudes, SR power, IR debris power, number of events per crossing, beam stability criteria and beam-stored energy were parametrized in terms of particle energy E, peak luminosity and arc bending radius ρ and plotted in the E/ρ plane for a given peak luminosity. This required to fix some of the parameters, such as β^*, the injection emittance ε_{inj}, the bunch spacing t_b, the bunch filling factor F, the number of interaction points (IP's) and the dipole filling factor PF in the arcs and the length of the straight sections l_s. Especially in what refers to beam-stability it was necessary to fix the lattice (transverse betatron amplitude $<\beta_t>$, synchrotron tune νs, fractional tune $\Delta\nu$) and the RF frequency (bunch length l_b at injection,..). In addition we assumed that this machine would be synchrotron radiation damped, thus it was stipulated that the luminosity beam lifetime (due to particle burn-off in the IP's) be longer than the radiation damping time. Furthermore the luminosity was specified to be at least $2 \cdot 10^{34} cm^{-2} sec^{-1}$, thus the boundary lines in the E/ρ plane are related to this luminosity only. The maximum luminosities in the possible island(s) in the E/ρ space were investigated separately. The formulas used in this context are described in the next section.

3.0 FORMULAS AND SCALING LAWS

3.1 Accelerator Parameter Calculation

The simulations for the different energy scenarios were calculated with the following set of equations (1)-(22). Specific references are omitted since these formulas are commonly used. They were recently compiled for example in [3] and [5].

The revolution frequency f_0 is calculated from the circumference Circ:

$$f_0 = \frac{c}{Circ} \quad (Hz) \tag{1}$$

The circumference is given by the arc bending radius ρ, the arc dipole filling-factor PF, and the length l_s of the straight sections:

$$Circ = 2l_s + \frac{2pr}{PF} \quad (m) \tag{2}$$

The average arc radius R is given with ρ/PF.
The relativistic factor gamma is calculated from the proton energy E_p:

$$g = \frac{E_p}{m_p c^2} \tag{3}$$

The injection energy is assumed to be determined by the collision energy E_p^{coll} and the dynamic range DR of the bending magnets. Henceforth the relativistic factor γ can be defined at collision or injection.

$$E_p^{inj} = \frac{E_p^{coll}}{DR} \tag{4}$$

The number of bunches N_b is calculated from the (fixed) bunch spacing time t_b, the revolution frequency f_0 and the bunch filling factor F (fraction of possible bunches filled):

$$N_b = \frac{F}{f_0 t_b} \tag{5}$$

The average beam current I_b is calculated from the number of bunches N_b and the number of protons per bunch N_{pb}:

$$I_b = f_0 e N_b N_{pb} \quad (Amp) \tag{6}$$

The guide field B (with the appropriate γ for the different cases of injection or collision) for a given bending radius ρ is:

$$B = \frac{m_p c g}{e r} \quad (T) \tag{7}$$

The proton-proton collision cross-section σ_{pp} is given as a linear extrapolation of literature data. E_{cm} is the center of mass energy ($2E_p$). The factor F_{inel}, the inelastic fraction, accounts for the irrelevance of small angle elastic scattering to beam loss. F_{inel} is assumed to be 0.734.

$$s_{pp} = (0.9 E_{cm}(TeV) + 18.45) \cdot F_{inel} \quad (mb) \tag{8}$$

The luminosity L (for round beams) is calculated from the number of particles per bunch N_{pb}, β^* and the normalized emittance ε_N. The number of particles per bunch N_{pb} and the normalized emittance ε_N are functions of time as a result of beam depletion due to collisions and radiation damping. A complication arises from the fact that N_{pb} (see (12)) depends on the time-integrated luminosity, making (9) an implicit equation for L.

$$L(L(t),t) = \frac{f_0 N_b g N_{pb}^2 (L(t))}{4\pi b^* \frac{eN(t)}{p}} \quad \left(\frac{1}{m^2 - \sec}\right) \tag{9}$$

At the peak luminosity in the presence of synchrotron radiation damping the emittance is usually damped to its minimum value ε_{Nmin} and the bunch intensity N_{pb} is reduced by a considerable amount, which both can vary on a case-to-case basis. Therefore it is very useful to have an approximate relationship between initial, L_{ini}, and peak luminosity, L_{peak}, allowing the derivation of the initial bunch population from a stipulated peak luminosity. The luminosity at injection L_{inj} can be easily related to the luminosity at the beginning of the store L_{ini} via the ratio of the γ factors at injection and full energy. Such a relationship in its simplest form is given in the following in terms of the constant Lfact and the dynamic range DR.

$$L_{ini} = \frac{L_{peak}}{Lfact} \quad L_{inj} = \frac{L_{ini}}{DR} \quad \left(\frac{1}{m^2 - \sec}\right) \tag{10}$$

The average luminosity over the store can be found from the time-integrated luminosity, normalized over a complete accelerator duty cycle, i.e. 2 ramps, the injection time and the store time. The magnet ramp rate is assumed to be 180 sec/T. The store time is assumed to be the time at which the average luminosity <L> peaks. Assuming a constant injection time t_{inj} (e.g. as in the case of a one-turn injection, t_{inj}~10 min), the average luminosity over the duty cycle becomes:

$$\langle L(t)\rangle = \frac{1}{t + t_{inj} + 2t_{ramp}(B)} \int_0^t L(t')dt' \quad \left(\frac{1}{m^2 - \sec}\right) \tag{11}$$

The luminosity lifetime τ_L, being a function of the number of particles in the beam and the luminosity, changes throughout the store as the number of particles diminishes and the luminosity varies. It is, however, sufficient for the purpose of this study to define a characteristic and constant luminosity lifetime as follows:

$$t_L = \frac{N_b N_{pb}^{ini}}{2 N_{ip} s_{pp} L^{peak}} \quad (\sec) \tag{12}$$

The number of particles per bunch N_{pb} is reduced during beam-beam collisions, according to (13), where the rate of particle burn-off depends on the integrated luminosity.

$$N_{pb}(L(t)) = N_{pb}(t_0) - \frac{N_{ip}}{N_b} s_{pp} \int_{t_0}^t L(t')dt' \tag{13}$$

The energy loss per particle per turn ΔE due to the emission of synchrotron radiation is:

$$\Delta E = \frac{4\pi r_p \gamma^4 m_p c^2}{3\rho} \quad (J) \tag{14}$$

The transverse radiation damping time τ_{rad} is a function of ΔE and the average arc radius R is:

$$t_{rad} = \frac{2E_p 2\pi R}{\Delta E\, c} = \frac{3R\rho}{r_p \gamma^3 c} \quad (\sec) \tag{15}$$

The emittance ε_N drops during radiation damping. A parametrization of the time dependence in terms of the radiation damping time and the initial and final emittances is given in (16). The final emittance is set by intra-beam scattering (IBS) and noise. These effects are neglected in this formalism and the emittance is allowed to damp down to the natural emittance e_{Nmin} (here denoted as $e_N(8)$) related to SR induced quantum excitation or the minimum emittance allowed for to agree with the beam-beam tune-shift limitation (9), whatever is larger.

$$eN(t) = eN(\infty) + (eN(t_0) - eN(\infty))e^{-\frac{2t}{t_{rad}}} \quad (m - rad) \tag{16}$$

The natural normalized transverse emittance e_{Nmin} in an isomagnetic ring with FODO lattice, as a function of energy, partition number J (J_{trans}=1), the dipole bending strength G (=1/ρ), and H, which depends on the lattice half-cell length $L_{1/2}$, is:

$$e_{N\min} = \frac{2.087 \cdot 10^{-16} g^3}{J_{trans}} \frac{\langle H \rangle}{r} \sim \frac{2.087 \cdot 10^{-16} g^3}{J_{trans}} \frac{C_h L_{1/2}^3 PF^2}{r^3} \quad (rad - m) \tag{17}$$

The beam-size can be derived from the normalized emittance with:

$$s_v = \sqrt{\frac{e_N b}{g}} \quad (m) \tag{18}$$

The SR power radiated by the beam can be calculated from the energy loss per proton per revolution ΔE, the number of protons in the ring $N_b N_{pb}$, the revolution frequency f_0 and the arc length 2πρ. The radiation power is largest at the beginning of the store when N_{pb} is largest.

$$p_{SR}^{peak} = \frac{\Delta E f_0 N_p}{2pr} = \frac{g^4 m_p c^2 4pr_p f_0 N_b N_{pb}^{ini}}{6pr^2} \quad \left(\frac{W}{m}\right) \tag{19}$$

The power carried by the collision debris into the IR, per beam, is largest at the peak luminosity:

$$p_{IR}^{peak} = E_p s_{pp} L^{peak} \quad (W) \tag{20}$$

The maximum number of events per crossing in the detector N_X can be calculated with:

$$N_X^{\max} = s_{pp} L^{peak} t_b \tag{21}$$

The stored energy per machine filling (beam) E_{beam} is maximal at the beginning of the store:

$$E_{beam}^{\max} = E_p N_b N_{pb}^{ini} \quad (J) \tag{22}$$

3.2 Beam-Stability Formulae

Simple formulas to estimate the beam stability limitations are given in (23)-(29).
The beam-beam tune-shift parameter (for round beams), which must remain below a certain threshold, depends on N_{pb} and ε_N and is thus as well changing during the store:

$$x = \frac{r_p N_{pb}(t)}{4p\,\frac{eN(t)}{p}} \tag{23}$$

The beam-beam tune-shift threshold depends on the damping decrement δ, i.e. the relative damping rate per turn, which in turn depends on the radiation damping time τ_{rad} (see 16) and the machine circumference Circ:

$$x_{\max} = 0.006 + 0.024\left(10^4 d\right)^{0.33} \tag{24}$$

$$d = \frac{c t_{rad}}{Circ} \tag{25}$$

The resistive wall instability rise-time is given in terms of the fractional tune-shift Δν, the thickness Δ and electrical conductivity σ of the beam-tube coating, the aperture-radius b, the number of particles per beam $N_b N_{pb}$ and the average betatron function $<\beta_t>$.

$$t_{RW} = \frac{pg\ \Delta n\ Z_0\ s\ \Delta b^3}{N_b N_{pb} r_p \langle b_t \rangle c} \quad (\text{sec}) \tag{26}$$

Since the rise-time is smallest at lower energy (~γ) the parameters should be evaluated at injection. The rise-time can be converted into an equivalent number of turns by multiplying with the revolution frequency.
The TMCI bunch-population threshold is a function of the synchrotron tune ν_s, the bunch length l_b, the average transverse β-function and the total transverse (high frequency) impedance $Z_\perp^{tot}$ in the ring. Again, the TMCI threshold is smallest at low energy and (27) should thus be evaluated at injection.

$$N_{TMCI} = \frac{32p^{3/2} n_s l_b \left(\frac{E_p}{e}\right)}{3ec\langle b_t \rangle Z_\perp^{total}} \tag{27}$$

The sum of the transverse impedance can be approximately found from the sum of the contributions by the bellows, BPM's, photon-stops, pumping holes and resistive wall. The transverse impedance of a shielded bellow / BPM is assumed to be 600 / 5000 Ω/m. The number of (shielded) bellows in the ring N_{bel} is assumed to be equal to the number of main magnets. The number of BPM's N_{BPM} is assumed to be the number of main quadrupoles. The number of photon-stops depends on the magnet aperture, arc bend radius and the specific scheme according to which the photon-stops are used (e.g. sharing radiation with beam-screen,..). The polarizability of the photon-stop α is πh^3, where h is the radial extension of the PS. The pumping hole impedance is given by the pumping hole width d_{ph}, the screen thickness t_{bs} and a correction factor F_{ph}(=0.56). The number of pumping holes N_{ph} depends on the machine size and on the pumping speed specified to

meet the vacuum requirements. Here a fixed number of pumping holes per meter ($N_h=n_h\cdot$Circ) and a fixed hole size is stipulated, assuming that the pumping speed requirements vary only weakly between different machines. The resistive wall impedance depends on the skin-depth, the bore radius b, the bunch-length frequency f_b ($f_b=c/l_b$, l_b is the bunch length), the revolution frequency f_{rev} and the machine circumference. Note that this calculation assumes photon-stops coexisting with a perforated beam-screen, as recently proposed for the VLHC in its second stage.

$$Z_{\perp}^{total} = N_{bel}\,600 + N_{BPM}\,5000 + N_{PS}\,\frac{aZ_0}{2p^2b^4} + N_{ph}\,\frac{Z_0 d_{ph} t_{bs}^3 F_{ph}}{2pb^4} + \frac{Circ^2 f_{rev}}{2p^{3/2}b^3}\sqrt{\frac{m_r Z_0}{csf_b}} \quad \frac{\Omega}{m} \tag{28}$$

The Laslett tune-shift is given in terms of the relativistic γ and β, the bunch intensity N_{pb}, the number of bunches N_b, the circumference Circ, the average transverse betatron amplitude in the arcs $<\beta_t>$, the normalized emittance ε_N, the bunch length l_b, the bore-radius b and the distance of the magnet pole faces (magnet yoke) from the beam d_p. As a rough approximation d_p is assumed to be 2b. As in the aforementioned cases the Laslett tune-shift is largest at injection and should thus be computed for this particular case.

$$dQ_L = \frac{r_p \langle b_t \rangle Circ N_{pb}}{b^2 g}\left\{\frac{1}{pl_b g^2}\left[\frac{g}{e_N\langle b_t\rangle}+\frac{p^2}{24b^2}\right]+\frac{b^2 N_b}{Circ}\left[\frac{p^2}{24b^2}+\frac{p^2}{12d_p^2}\right]\right\} \tag{29}$$

3.3 Scaling Laws

The set of equations listed in 3.1) can be used to simulate possible accelerator scenarios. Trial and error methods or numerical programs can be used to obtain scenarios that satisfy the constraints discussed in 2). To obtain general rules that delimit the areas in any arbitrary parameter space that satisfy the above listed constraints, scaling laws have to be formulated, that can involve a number of simplifications. The following lists such scaling laws in the energy/luminosity/bending radius space for the restricted parameters listed above, namely p_{SR}, p_{IR}, N_X, E_{beam}, ?, τ_{RW}, N_{TMCI} and δQ_L. The simplifications are manifold: first a certain number of parameters were held constant, they are described in Table 1. Second, the complex patterns of interdependencies between the different parameters, were as much as reasonably possible, suppressed. The following describes the scaling laws and explains the simplifications that were introduced.

The peak synchrotron radiation power (19) depends on the particle energy, the initial average beam current (6) and the arc-bending radius. The beam current can be reformulated in terms of the luminosity (9). The luminosity varies strongly throughout the store and with it the SR power. As a simplification the SR power in (30) is calculated at the time when the luminosity peaks. This simplification is especially useful because it implies that the emittance, which enters the power law through the luminosity can easily be defined via the beam-beam tune-shift limit. In synchrotron radiation damped machines, at the early plateau when the luminosity reaches its peak, the emittance is usually damped. As discussed before, the emittance damping can usually not be allowed

to proceed to the “natural emittance level” (17). Rather, the beam-beam tune-shift limitation requires a heating of the emittance to a level that is somewhat larger than the natural emittance. Therefore, the SR power law (30) represents rather the average SR power than the peak power (which is radiated at the beginning of the store). On the other hand (30) becomes a good approximation of the peak power in cases in which the radiation damping time is short enough, i.e. in synchrotron radiation dominated machines. As was mentioned before and will be discussed later in this note, the condition that the radiation damping time is short enough is always presupposed in this study. The beam-beam tune-shift parameter ? is a function of the damping decrement and thus depends on ~$\rho^{1/3}/\gamma$. In (30) ? has been assumed constant (?=0.008) which is accurate for damping decrements in the range 10^{-6} to 10^{-8}, which covers a large range of possible machines and especially those that are SR dominated.

$$p_{SR}^{av} = \frac{4\pi r_p^2 b^* }{\left(m_p c^2\right)^2 6\pi x} \frac{L^{peak} E_p^3}{r^2} = C_{SR}\left(b^*, x\right) \frac{L^{peak} E_p^3}{r^2} \quad \left(\frac{W}{m-beam}\right) \tag{30}$$

(30) resembles strongly (19) except that one power in E and the beam current dependence are replaced by the luminosity . The beam-beam tune-shift parameter, which compensates one order of the bunch population in the luminosity, is buried in the C_{SR} constant.
The IR debris power (20) is easily written in terms of luminosity and energy with the cross-section fit (8).

$$p_{IR}^{peak} = 1.8 \cdot 10^{-31} F_{ie} E_p^2 L^{peak} + 18.45 \cdot 10^{-31} F_{ie} E_p L^{peak} = C_{IR1}\left(F_{ie}\right) E_p^2 L^{peak} + C_{IR2}\left(F_{ie}\right) E_p L^{peak} \quad (W)$$

(31)

Thus the IR peak-power limitation is soft, in the sense that it can be moved to higher energies by reducing the luminosity.
The scaling law for the maximum number of events per crossing (21) is similarly straightforward:

$$N_X^{\max} = 1.8 \cdot 10^{-31} F_{ie} t_b E_p L^{peak} + 18.45 \cdot 10^{-31} F_{ie} t_b L^{peak} = C_{X1}\left(t_b, F_{ie}\right) E_p L^{peak} + C_{X2}\left(t_b, F_{ie}\right) L^{peak}$$

(32)

The average total beam energy scaling law can as well easily be adapted from (22) by replacing current by the peak luminosity and the max beam-beam tune-shift parameter in a way similar to that employed in the case of the SR power. Similar arguments as in the case of the SR power – average versus peak – apply as well in this case.

$$E_{beam}^{av} = \frac{b^* r_p m_p c^2}{\pi x f_0} L^{peak} = C_{Eb1}\left(b^*, x, l_s\right) L^{peak} + C_{Eb2}\left(b^*, x, PF\right) \rho L^{peak} \quad (J) \tag{33}$$

Interestingly the particle energy does not explicitly appear in (33). The luminosity function (9) contains one order of energy, but for a fixed luminosity the energy dependence vanishes completely. This is related to SR damping. As the particle energy gets higher, the emittance shrinks due to damping, such that the beam current has to be reduced to keep the luminosity constant. Therefore, at fixed luminosity the total energy product in the beam has to stay constant.
The condition that the radiation damping time is smaller or equal than the luminosity lifetime can be implemented with (12) and (15). As before in the case of the SR power and the beam energy, the beam-beam tune-shift condition is introduced into the equation via the bunch population or the luminosity, respectively. Therefore (34) computes the peak damping time ratio at peak luminosity. Another simplification made, is the omission of the length of the straight sections in the circumference in $C_{\tau 1}$ and $C_{\tau 2}$.

$$\frac{t_{rad}}{t_L}^{peak} \approx \frac{6N_{ip}x\left(m_p c^2\right)^2}{2pr_p^2 b^*}\frac{s_{pp}r}{E^2} = C_{t1}\left(N_{ip},x,b^*\right)\frac{r}{E} + C_{t2}\left(N_{ip},x,b^*\right)\frac{r}{E^2} \tag{34}$$

As expected, (34) demands a large particle energy and a small bending radius in order to maximize SR emission. The beam-current is contained in $C_{\tau 1}$ and $C_{\tau 2}$ via the beam-beam tune-shift parameter.
Although the beam-beam tune-shift parameter (23) is taken into account in the synchrotron radiation scaling law (30), it makes sense to introduce a separate beam-beam tune-shift scaling law. This law limits the luminosity only in low energy, low synchrotron radiation power level cases, in which the beam current has to be very high to achieve high luminosity.

$$z_{\max} = r_p\sqrt{\frac{b^* t_b\left(m_p c^2\right)}{4Fe_{Ninj}}}\sqrt{\frac{L^{peak}}{E}} = C_x\left(t_b, b^*, F, e_{Ninj}\right)\sqrt{\frac{L^{peak}}{E}} \tag{35}$$

The resistive wall e-folding time (26) depends mainly on the magnet aperture, injection energy, the beam-current and the thickness of the beam-tube (copper) coating. The scaling law (36) applies to the number of turns N_{RW} related to the characteristic e-folding time ($N_{RW}=\tau_{RW}f_{rev}$). For the scaling law the magnet aperture, coating thickness and RRR, lattice parameters ($\Delta\nu$, $<\beta_{tinj}>$) were fixed. The initial luminosity and injection particle energy are related to the peak luminosity and the collision energy through (10) and (4). As a simplification the circumference was approximated with $2\pi\rho/PF$ instead of using the complete formula (2). Furthermore the magnetic field in the Cu-conductivity function σ was fixed to a constant value (B_{inj}), to allow inclusion of σ in C_{RW}.

$$N_{RW} = \frac{p\,\Delta n\,Z_0\,s_{Cu}\left(T, B_{inj}, RRR\right)c\Delta b^3\sqrt{Lfact}}{2^3\sqrt{\frac{F}{t_b}}r_p\left\langle b_{tinj}\right\rangle\left(m_p c^2\right)^{3/2}DR\sqrt{4pb^*\frac{eNinj}{p}}\left(\frac{2p}{PF}\right)^2}\frac{E_p^{3/2}}{r^2\sqrt{L^{peak}}} =$$

$$C_{RW}\left(\Delta n, b, \Delta, Lfact, DR, b^*, e_{Ninj}, PF, T_{bs}, B_{inj}, RRR_{Cu}, \left\langle b_{tinj}\right\rangle, t_b, F\right)\frac{E_p^{3/2}}{r^2\sqrt{L^{peak}}} \tag{36}$$

Because of the complexity of expression for the sum of the transverse impedances, the scaling law for the TMCI threshold can only be obtained numerically, setting the bunch population to N_{TMCI} (27) in the luminosity definition in (9).

$$\sqrt{\frac{4pb^*\frac{e_N}{p}L^{peak}\left(m_p c^2\right)}{\frac{F}{t_b}E_p^{coll}\;Lfact}} = N_{TMCI} = \frac{32p^{3/2}n_{\sin j}\frac{l_{binj}}{2\sqrt{2p}}\left(\frac{E_p^{coll}}{e}\right)}{3ec\left\langle b_{tinj}\right\rangle Z_\perp^{total}(b, r)DR} \tag{37}$$

The Laslett tune-shift scaling law stated explicitly in terms of E_p, ρ and L is given in (29). The initial bunch intensity N_{pb} in (29) is expressed in terms of the peak luminosity using (9) and (10), the circumference was replaced by $2\pi\rho/PF$. The relativistic β is assumed to be ~1 in (38). The pole distance is written in terms of the bore radius with d=2b.

$$dQ_L = \frac{r_p\left\langle b_{tinj}\right\rangle\sqrt{4pb^*\frac{e_{Ninj}}{p}L^{peak}}Circ(r)}{\sqrt{\frac{F}{t_b}\;Lfact\,DR\,b^2 g_{inj}^{3/2}}}\left\{\frac{1}{pl_{binj}g_{inj}^2}\left[\frac{g_{inj}}{e_{Ninj}\left\langle b_{tinj}\right\rangle}+\frac{p^2}{24b^2}\right]+\frac{b^2F}{t_b c}\frac{3p^2}{48b^2}\right\} =$$

$$= C_{LTS1}\left(\left\langle b_{tinj}\right\rangle, b^*, e_{Ninj}, l_{binj}, L_{fact}, t_b, DR, PF\right)\frac{\sqrt{L^{peak}}\,r}{E_p^{5/2}} +$$

$$C_{LTS2}\left(\left\langle b_{tinj}\right\rangle, b^*, e_{Ninj}, l_{binj}, L_{fact}, t_b, DR, PF, b\right)\frac{\sqrt{L^{peak}}\,r}{E_p^{7/2}} +$$

$$C_{LTS3}\left(\left\langle b_{tinj}\right\rangle, b^*, e_{Ninj}, L_{fact}, t_b, DR, PF, b\right)\frac{\sqrt{L^{peak}}\,r}{E_p^{3/2}} \tag{38}$$

4.0 RESULTS

4.1 Parameter Tables

The quantitative choices for the fixed parameters in the exploration of the parameter space of very large hadron colliders is the subject-matter of chapter 2. They are listed in Table 1. A brief justification of the numbers chosen is given in the following.

The straight section length of 10 km is generous, but it is a fair approximation in the very high center-of-mass energy range. The dipole packing factor of 85% is typical of a FODO lattice. The dynamic range of 10 is similarly more typical of a high field magnet ring. The luminosity enhancement factor is a purely mathematical entity, and not further discussed here. The bunch filling factor describes the number of filled bunches, out of those that can possibly be filled. A bunch spacing time of 12 ns requires a RF frequency of ~80 MHz. A betastar of 30 cm was recently proposed for the VLHC-1. The average betafunction (163 m) is applicable to both stages of the currently proposed VLHC and therefore considered to be a very general choice. The choice of the magnitude of the injection emittance, for example, is typical for a non radiation-damped injector. The physical beam tube aperture of 20 mm is certainly smaller than in any other hadron accelerator before. The smaller aperture reflects the trend of reducing the aperture in the presence of more energetic and focused beams. The beam screen temperature is high, reflecting the need to limit the plug-power requirements of beam screens extracting high synchrotron radiation heat loads. The beam-tube coating thickness of 200 μm is compatible with quench force limitations in 10 T superconducting magnets.

Table 1: Fixed Parameters in accelerator simulations.

Parameter	*Fixed Value*
Number of IP's	2
Length of straight sections l_s (km)	10
Dipole packing factor PF	0.85
Dynamic range DR	10
Luminosity enhancement factor L_{fact}	5
Bunch filling factor F	0.9
Bunch spacing time (ns)	12
Betastar β^* (m)	0.3
Average transverse β function at injection $<\beta_{tinj}>$ (m)	163
Normalized injection emittance ε_{inj} (μm)	1.5·p
Synchrotron tune at injection ν_s	0.1
Rms bunch length at injection l_b (cm)	8.2
Fractional tune-shift $\Delta\nu$	0.1
Beam-beam tune-shift parameter ?, when fixed	0.008
Magnet aperture ∅ 2b (mm)	20
Beam screen temperature T_{bs} (K)	100
Beam screen coating RRR	100
Beam screen coating thickness Δ (μm)	200
Number of pumping holes in beam-screen per m n_h	120
Dimensions of pumping hole in beam-screen (mm x mm)	1.5 x 8
Injection field in conductivity function B_{inj} (T)	1

The scaling law constants are conveniently expressed in units of TeV, km and 10^{34}/cm^2/sec, so that the energy, bending radius and luminosity can be used in these practical magnitudes.

Table 2: Constants used in the Scaling Laws.

Constant	Value	Unit
$C_{SR}(\beta^*,?)$	0.00107	$W/m\cdot(km^2)/(TeV^3)/(10^{38}m^{-2}s^{-1})$
C_{IR1}	2.133	$W/(TeV^2)/(10^{38}m^{-2}s^{-1})$
C_{IR2}	21.696	$W/(TeV)/(10^{38}m^{-2}s^{-1})$
$C_{X1}(t_b)$	0.16	$1/(TeV)/(10^{38}m^{-2}s^{-1})$
$C_{X2}(t_b)$	1.625	$1/(10^{38}m^{-2}s^{-1})$
$C_{Eb1}(\beta^*,?,l_s)$	57.7	$MJ/(10^{38}m^{-2}s^{-1})$
$C_{Eb2}(\beta^*,?,PF)$	21.33	$MJ/km/(10^{38}m^{-2}s^{-1})$
$C_{t1}(N_{ip},?,\beta^*)$	$4.067\cdot10^{-7}$	TeV/km
$C_{t2}(N_{ip},?,\beta^*)$	25.825	TeV^2/km
$C_?(t_b,\beta^*,F,\varepsilon_{Ninj})$	0.00685	$(TeV)^{1/2}/(10^{38}m^{-2}s^{-1})^{1/2}$
$C_{RW}(\Delta\nu,b,\Delta,L_{fact},DR,PF,T_{bs},B_{inj},<\beta_{tinj}>\beta^*,\varepsilon_{Ninj},F,t_b)$	5.258	$km^2(10^{38}m^{-2}s^{-1})^{1/2}/(TeV)^{3/2}$
$C_{LTS1}(l_{binj},t_b,L_{fact},DR,<\beta_{tinj}>,\beta^*,\varepsilon_{Ninj})$	$9.8\cdot10^{-5}$	$(TeV)^{5/2}/km/(10^{38}m^{-2}s^{-1})^{1/2}$
$C_{LTS2}(l_{binj},t_b,L_{fact},DR,b,<\beta_{tinj}>,\beta^*,\varepsilon_{Ninj})$	$2.9\cdot10^{-7}$	$(TeV)^{7/2}/km/(10^{38}m^{-2}s^{-1})^{1/2}$
$C_{LTS3}(l_{binj},t_b,L_{fact},DR,b,<\beta_{tinj}>,\beta^*,\varepsilon_{Ninj})$	$3.2\cdot10^{-2}$	$(TeV)^{3/2}/km/(10^{38}m^{-2}s^{-1})^{1/2}$

Table 3 resumes the accelerator physics limitations of hadron colliders. The parameters are discussed in detail in part 2).

Table 3: Limiting Parameters used in the Energy/Luminosity Scaling Study.

Parameter	Limit
Average synchrotron radiation power (W/m/beam)	5
Peak synchrotron radiation power (W/m/beam)	~10
Peak IR debris power (kW/beam)	50
Maximum number of events per crossing	60
Maximum beam-beam tune-shift parameter	0.008
Maximum peak beam stored energy (GJ)	10
Ratio of radiation damping and luminosity lifetime -peak	0.5
Ratio of radiation damping and luminosity lifetime -average	~1
Resistive wall instability rise-time (turns)	1
Initial bunch intensity given by TMCI criterion	N_{TMCI}
Maximum Laslett tune-shift	0.2
Minimum luminosity $\cdot10^{34}$ cm^{-2}s^{-1}	2

4.2 SR and IR Debris Power

The scaling laws (30)-(38) were evaluated, using the fixed parameters and constants listed in Table 1 and Table 2 and the limitations listed in Table 3, to obtain the limiting bounds of accelerator operation in the plane of particle energy and arc bending radius. Figure 1 shows the results (excluded beam-stability criteria). The luminosity in the scaling laws was fixed to $2 \cdot 10^{34} cm^{-2} s^{-1}$ and therefore the limiting lines refer to this luminosity only. The following observations can be made:

- The "possible" region is contained in a band in the energy/radius plane, which is delimited toward higher energies by the SR power and at the low energy bound by the "minimum SR" requirement, formulated via the ratio of luminosity lifetime and SR damping time. The width of this band is determined by the choice of the SR power limitation.
- A closer look shows, that for the given choice of magnitude for the limiting parameters, the upper boundary of the possible region is not SR power, but magnet technology below 100 TeV particle energy and 22 km of guide field bending radius (assumed to be currently limited to 15 T in the most optimistic scenario) and IR debris power for machines operating with bending radii larger than 22 km.
- The 50 kW/beam IR debris power limitation sets a machine size independent limit of ~100 TeV per particle, if the $2 \cdot 10^{34}$ $cm^{-2} sec^{-1}$ luminosity level is to be up-held.
- The chosen limitation on the number of events per crossing turns out to be a "softer" limit than the IR debris power limit. Thus, if a machine satisfies the IR power limit it will in general not conflict with the 60 events per crossing limitation. A parameter, which can drastically alter this conclusion is the bunch spacing time (currently set to 12 ns).
- The machines operating below the SR damping condition are not necessarily excluded. They do not operate in the SR dominated regime and can therefore not take advantage of SR damping to achieve high luminosities (and use high beam currents instead). There may be other compelling reasons, e.g. reduced magnet cost as in the current proposal for the VLHC-1 [3], that justify such a choice. In this study however, these options were not considered.
- The total beam-energy limitation to 10 GJ, at a peak luminosity of $2 \cdot 10^{34}$ $cm^{-2} sec^{-1}$, excludes machine designs with arc bending radii beyond ~200 km, which is by far outside of the range investigated here. At higher luminosities, however, this machine size limit becomes important (see 4.8).

The calculated luminosities in the "allowed" region, corresponding to the case discussed here are shown and discussed in 4.5. The beam stability limitations are shown in 4.3. A summary of only the most stringent limitations is given in 4.4.

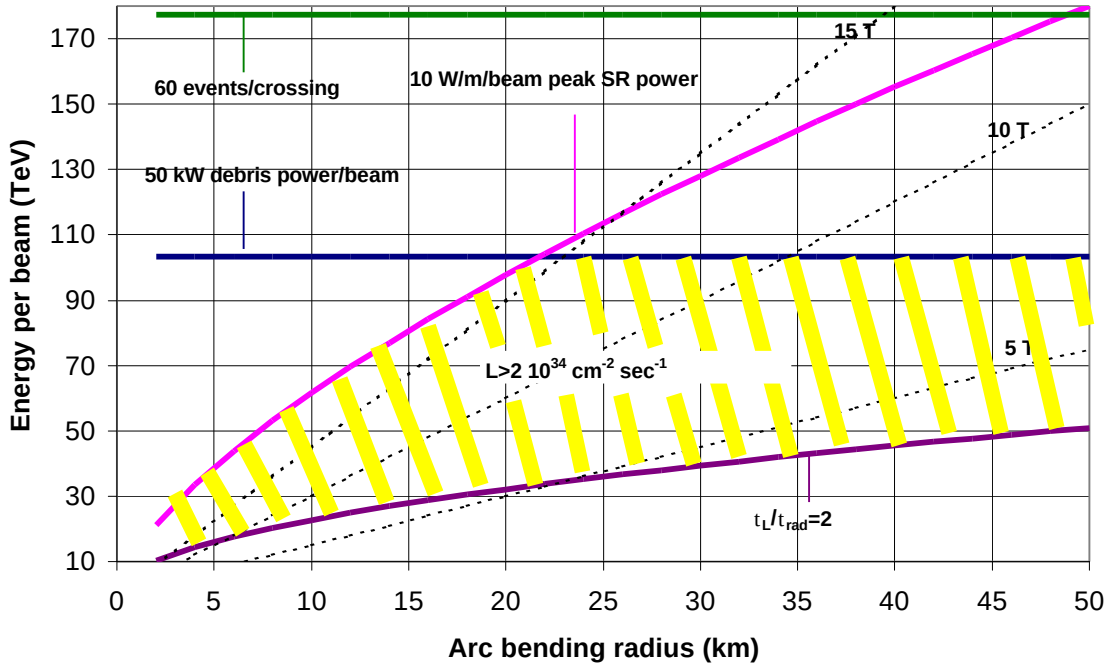

Figure 1: "Allowed" energy/radius combinations for future proton colliders (hatched area) taking into account IR power, SR power and number of events per crossing limitations. The lowest line represents the minimum condition for synchrotron radiation damping. Shown are as well the lines for bending fields of 5, 10 and 15 T.

4.3 Including Beam Stability

The dominant beam instabilities in the VLHC are of the transverse type. They depend strongly on the magnet aperture. All of the instabilities depend on the beam current in some way; so improved emittance (and therefore fewer protons needed to reach the desired luminosity) would improve the situation. Figure 2 shows the beam-stability boundaries in the E/ρ space at a minimum luminosity of $2 \cdot 10^{34}$. As indicated in the figure the excluded area lies below the curves, toward lower energy, the "hatched" area being that above the beam stability thresholds. The figure shows the most important beam-instabilities, resistive wall instability, Laslett tune-shift, TMCI and beam-beam tune-shift. Note that the beam-beam tune-shift is included in all limiting curves in Figure 1. Note as well that the boundaries shown here apply to a 20 mm beam-pipe aperture, a beam-tube operated at 100 K, with a 200 μm Cu coating (see Table 1). This level of aperture has to be considered small compared to that in the LHC or SSC magnets. It is nevertheless believed to be a realistic choice and being proposed in the recent VLHC study [3]. Although the lines in Figure 2 are drawn in the collision energy / ρ plane, the stability criteria were calculated at injection energy and converted into equivalent collision energies assuming a dynamic range of 10 for the magnets.

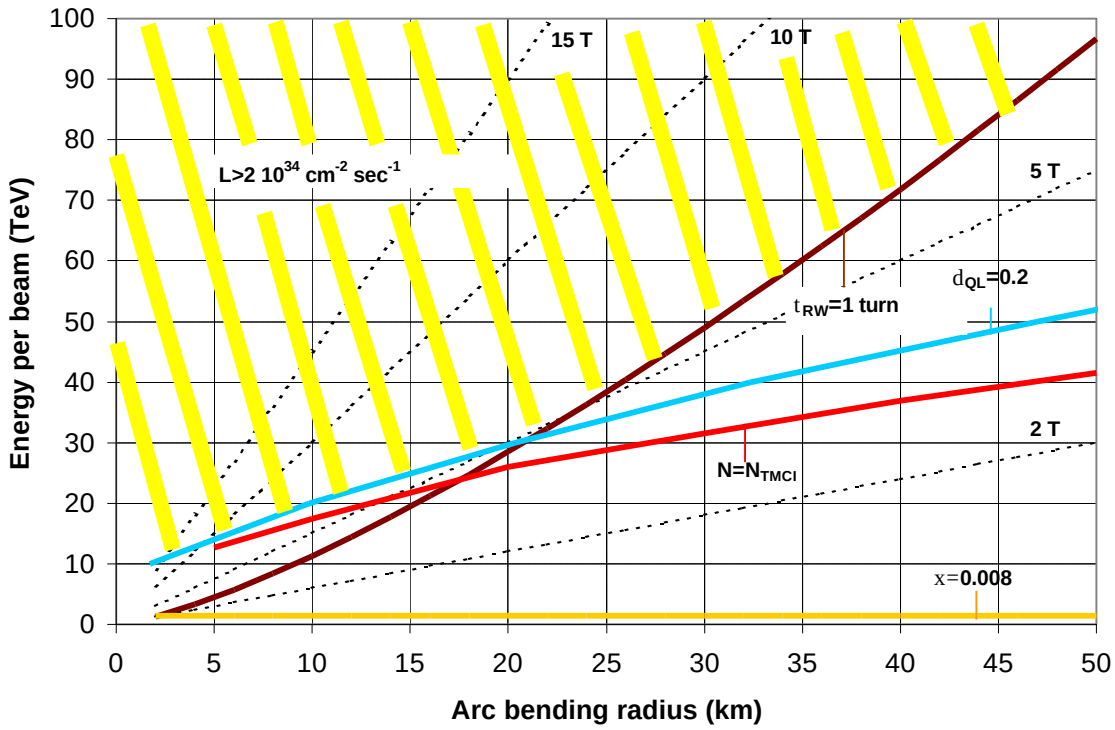

Figure 2: Possible particle energy/machine size combination for future proton colliders (hatched area), taking into account beam-stability only.

Figure 2 clearly shows that beam stability issues limit accelerator performance at low particle energy and large ring size. It appears that beam stability is a soft limitation however, because even cases above the thresholds can be handled with a combination of actions, including feedback systems of moderate power and bandwidth; increasing the number of bunches at injection and coalescing the beam at higher energy; reducing the beam emittance with an improved injector chain or increased injection energy; or by increasing the beam tube diameter and the magnet gap. The first stage of the current VLHC proposal [3] is exactly such a machine, where appropriate measures allow operation above the beam-stability thresholds.

4.4 The "Allowed" Region

Figure 3 combines Figure 1 and Figure 2, keeping only the most stringent delimitations of the possible accelerator space. Existing proposals for a VLHC (SSC, VLHC-Snowmass 1996 version and the latest VLHC proposals) are shown. The term "allowed region", should not be taken too seriously because the delimited area in the E/ρ space depends strongly on the particular choice for the fixed parameters and limits.

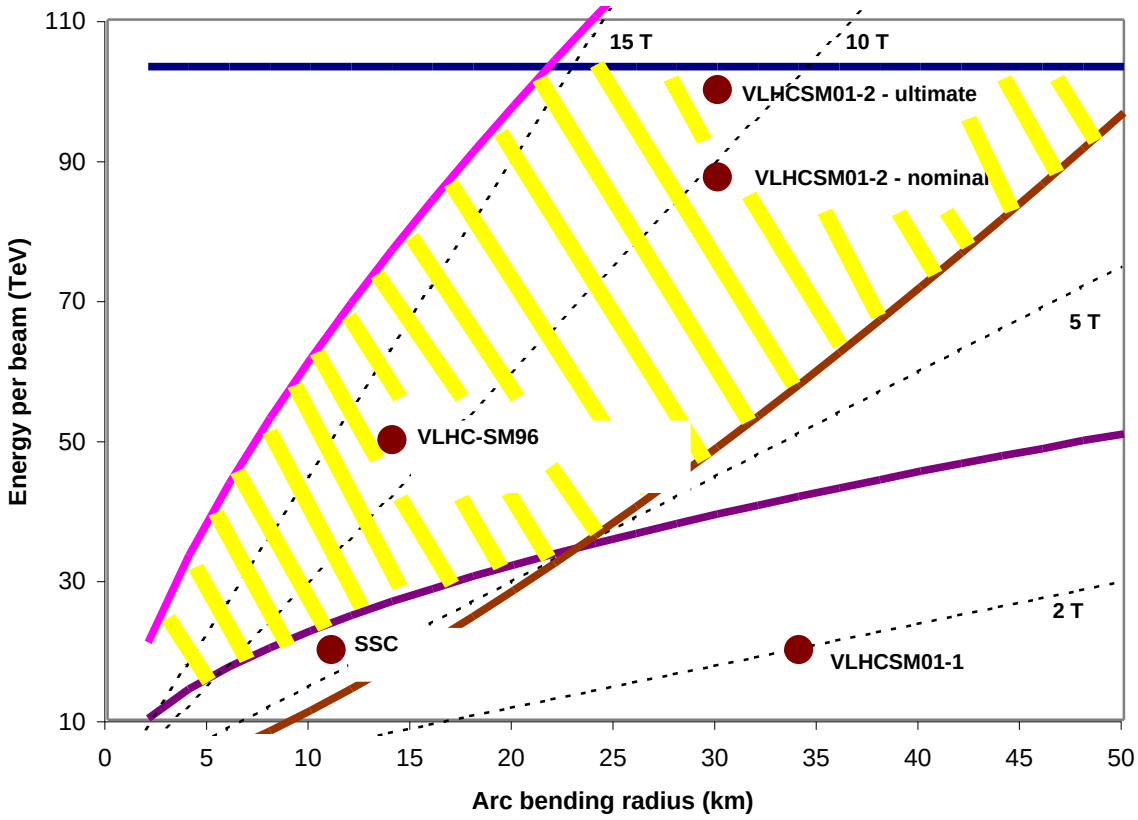

Figure 3: Possible particle energy/machine size combination for future proton colliders (hatched area). The most relevant limitations from Figure 1 and Figure 2 are retained in this plot. They are: IR power, SR power, Laslett tune shift and resistive wall instability. Shown are as well the operating points for existing VLHC proposals [3]. "SM01" stands for Snowmass 2001, etc..

Table 4 - Table 6, in the appendix, resume detailed calculations of VLHC scenarios using the set of formulas (1)-(29). The calculations used the fixed parameters listed in Table 1 and aimed at staying within the constraints listed in Table 3. Figure 4 plots the points in the E/ρ space that were simulated.

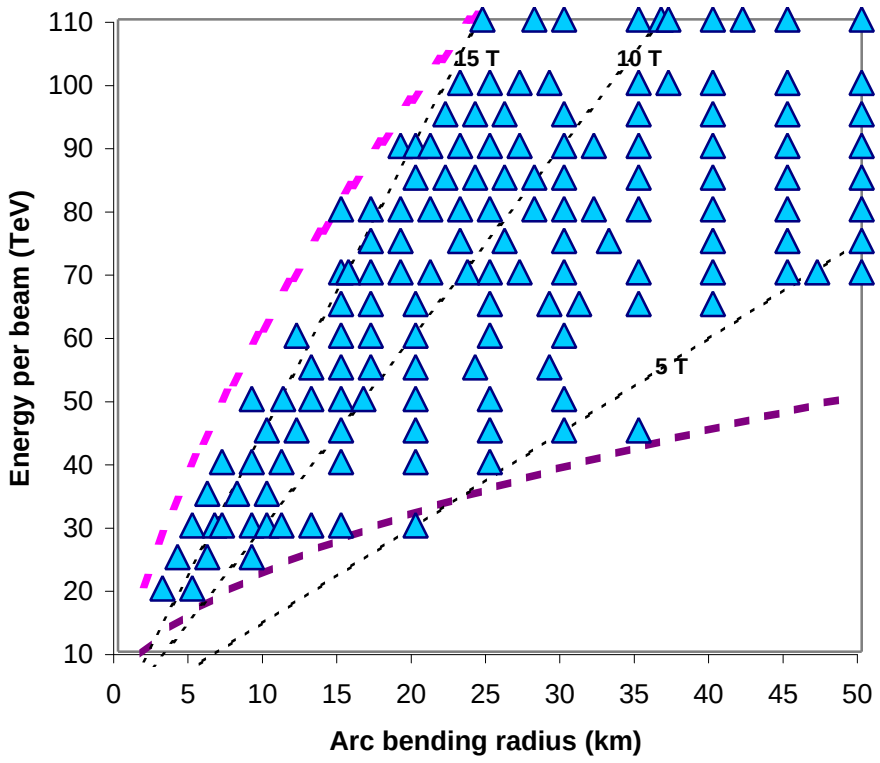

Figure 4: Possible particle energy/machine size combination for future proton colliders (hatched area). Shown are the simulated solutions listed in Table 4, Table 5 and Table 6.

4.5 Luminosity Profile I

The luminosity in the "permitted" region was calculated and the results are shown in Figure 5. The region of highest luminosity appears in the middle of the "band" delimited by the SR power and the minimum radiation damping. This can be explained by damping: The further above the minimum damping boundary the larger the luminosity as a result of damping. At the same time the radiation power rises, such that the luminosity (or the beam current) has to be lowered again as one approaches the upper SR-power boundary. At the boundaries of the possible region the luminosity is per definition fixed to $2 \cdot 10^{34} cm^{-2} s^{-1}$. Furthermore the maximum luminosity has to decrease as one goes to higher energy because of the strong energy dependence of the SR power. As mentioned before, beam-stability (except beam-beam tune-shift) was not taken into account in the luminosity calculations shown in Figure 5. Figure 5 shows that a luminosity of $10^{35} cm^{-2} s^{-1}$ can only be achieved at lower particle energy and using very high field magnets. In fact the region of highest luminosity is following a line crossing through the plane from very high fields at small machine radii to medium fields at large machine circumference. For 85 TeV per beam the highest achievable luminosity appears at 9 T. In Figure 5 the line of maximum luminosity is truncated at large machine sizes because of the IR debris limit and, secondary in importance, the number of events limit. This conclusion, however, is

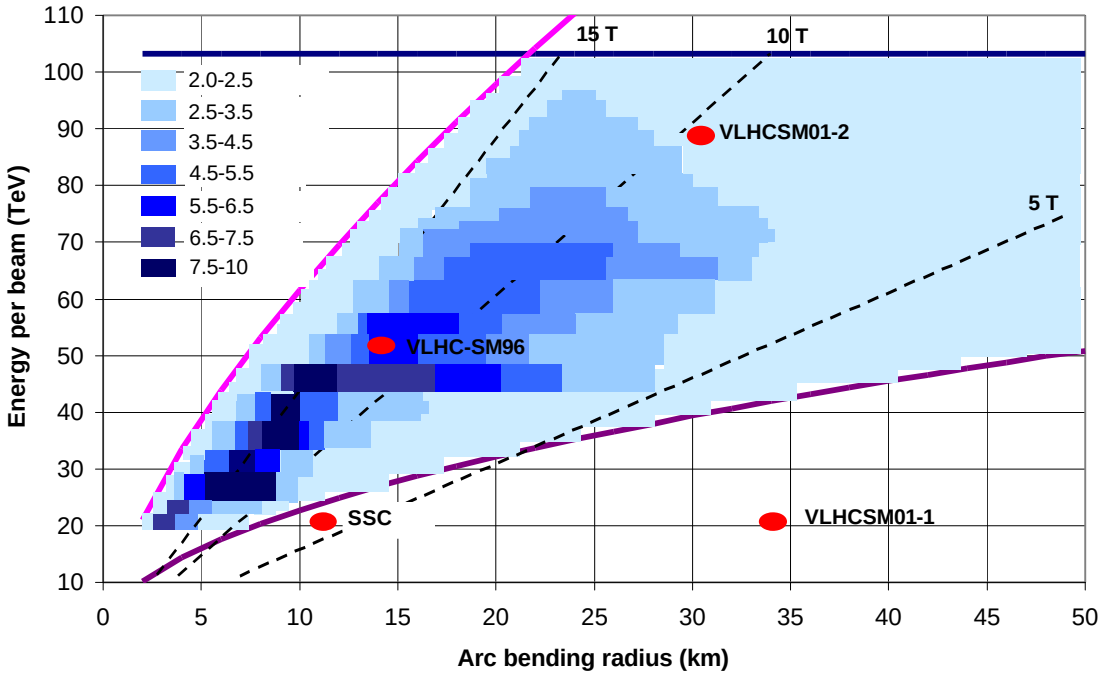

Figure 5: Maximum Luminosity in the "possible" region of VLHC accelerator space, in units of 10^{34}cm^{-2}s^{-1}. Beam-beam parameter, SR-power, IR-power, number of event limits, as stated in Table 3, are respected.

strongly tied to the set of limiting parameters chosen here. If a larger IR debris power than 50 kW/beam can be tolerated, for example, the luminosities achievable for 100 TeV protons can as well reach up to 10^{35} cm^{-2}s^{-1}. Obviously a larger synchrotron radiation power limit (larger than 10 W/m/beam at peak) would allow larger luminosities, moving the luminosity maximum toward higher field magnets. The currently proposed VLHC in its ultimate stage with 200 TeV center of mass energy finds itself close to the edge of the $2{\cdot}10^{34}$ luminosity region. The accelerator simulations on which Figure 5 is based are summarized in Table 4.

4.6 Luminosity Profile II

Figure 6 shows the peak luminosities that can be achieved in VLHC if only the SR-power and beam-beam limits are taken into account. As expected the luminosities are stratified along lines parallel to the SR-power limit, becoming larger the further away from the SR limit boundary. The very high luminosities in the region of large ρ and at low energy are actually limited by the beam-beam parameter. The minimum synchrotron radiation damping condition leads to a sudden (and artificial) drop in luminosity at the minimum damping condition boundary.

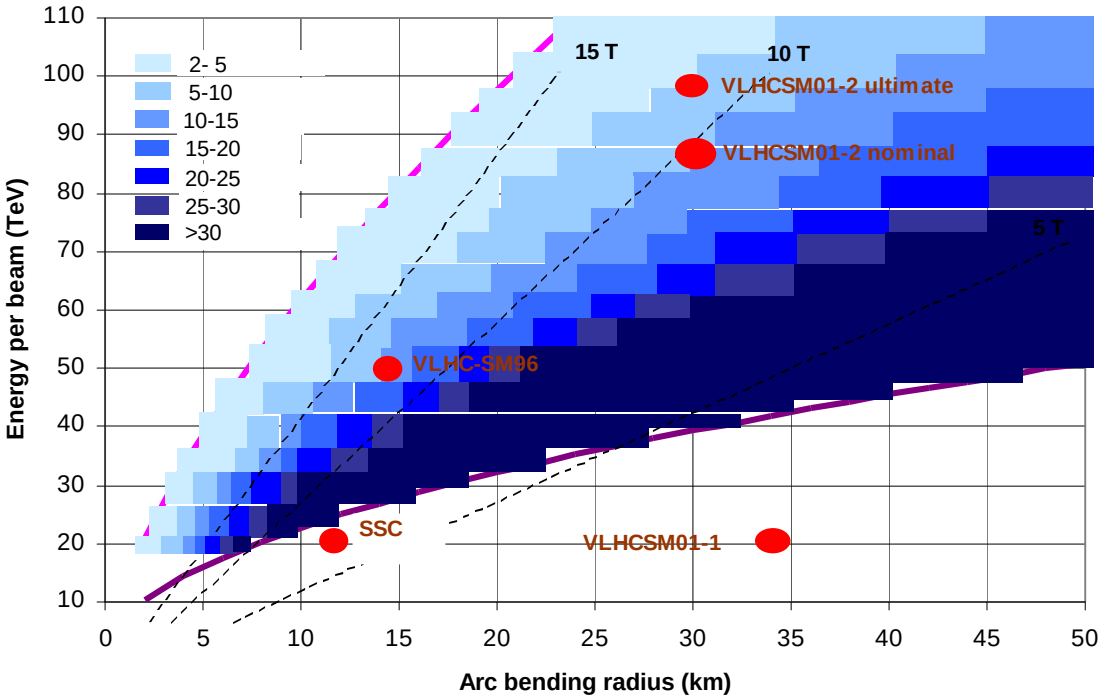

Figure 6: **Maximum Luminosity in the "possible" region of VLHC accelerator space, in units of $10^{34}cm^{-2}s^{-1}$(color code). Only SR-power and beam-beam limits, as stated in Table 3, are respected.**

4.7 Luminosity Profile III

Figure 7 essentially reproduces the case presented in 4.6, except that beam stability is taken into account, which excludes the extreme luminosity solutions found at the lower boundary of the analyzed region. Still, as in the former case, no IR-power or number of events limit was taken into account. The result shows that the highest luminosities can be found along a line going from very high fields (15 T) at lower energy (40 TeV per beam) to high fields (9 T) at 70 TeV per beam, to moderate fields (8-9 T) at 100 TeV per beam. Figure 5 can be obtained from Figure 7 by reducing the maximum luminosities in machines with a bend-radius larger than ~20 km as a result of the IR power limitation. As mentioned numerous times before the line of maximum luminosity can easily be moved, for example toward smaller fields if the beam-stability conditions can be relaxed (larger magnet bore, applying correction schemes,.etc.) or toward larger fields if the SR-power limit is raised.

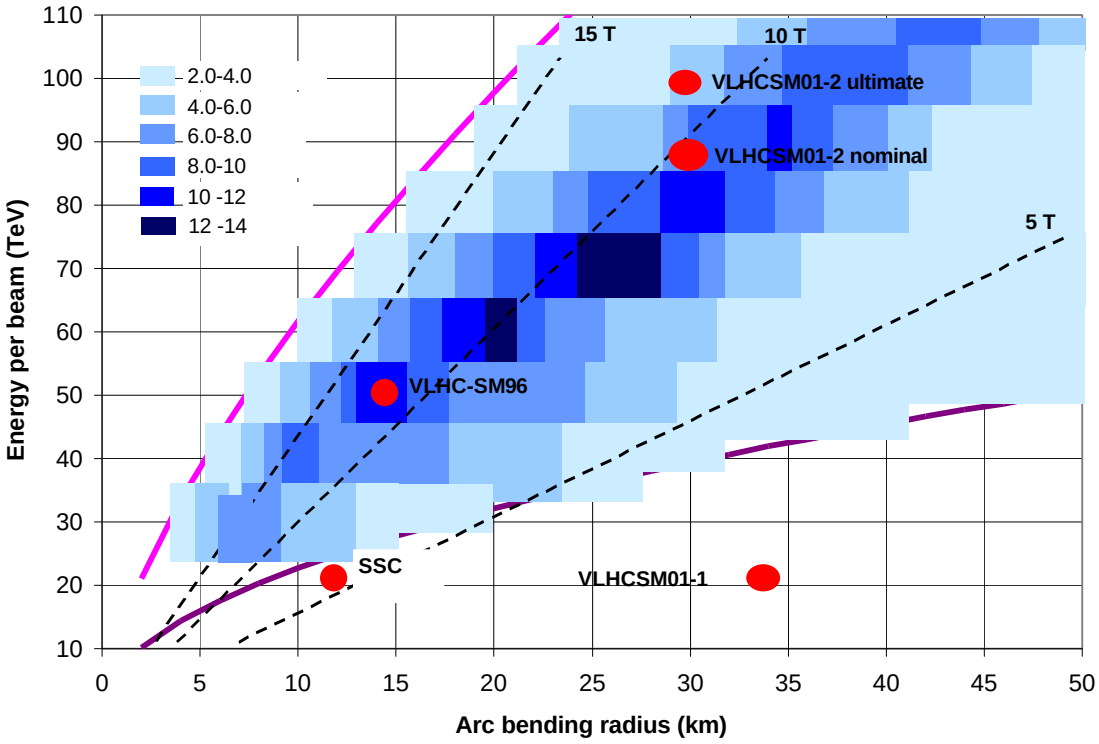

Figure 7: Maximum Luminosity in the "possible" region of VLHC accelerator space, in units of $10^{34}cm^{-2}s^{-1}$. Only SR-power and beam-beam limits, as stated in Table 3, are respected.

4.8 Stored Beam Energy Limitation

At a luminosity of $2 \cdot 10^{34}$, the beam energy limit, set to 10 GJ at the peak, is not of concern. But, as shown in Figure 8, the higher the luminosity the smaller the machine must be to remain within the beam-stored energy limit. The beam-energy limit was not taken into account in the calculations leading to Figure5-Figure7, though it would somehow alter the picture, setting a limit to luminosity in larger machines (especially in the case of Figure 6, but as well in the case of Figure 7). Figure 8 shows the limiting machine radius as a function of peak luminosity for an average beam energy of 5 GJ (~peak beam energy of 10 GJ).

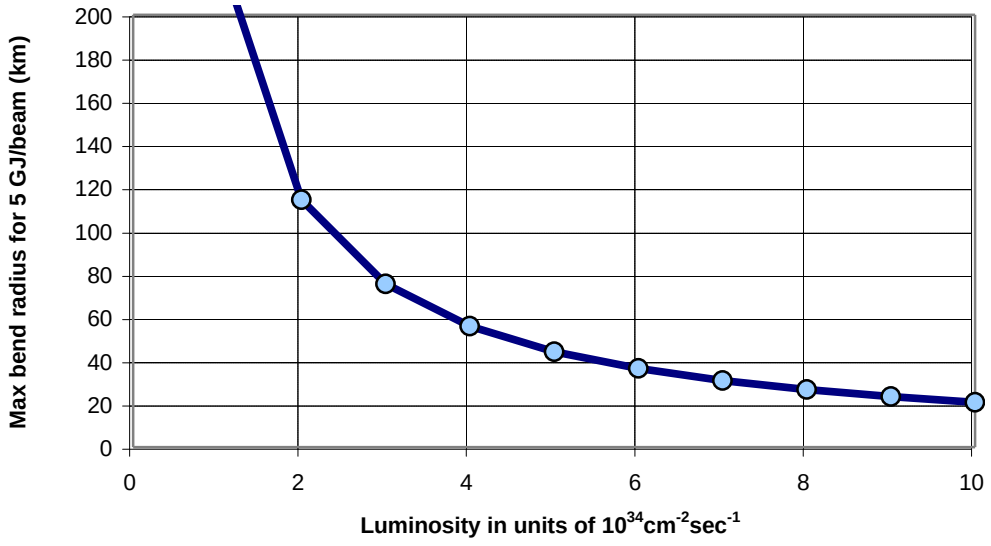

Figure 8: Maximum bend radius compatible with a 5 GJ average stored beam energy limit.

5.0 CONCLUSIONS

Future hadron colliders, especially in regimes with particle energies in excess of 40 TeV per proton will most likely be synchrotron radiation dominated. Assuming limits for the synchrotron radiation power, the IR debris power, the maximum number of events per crossing and demanding that there be enough synchrotron radiation to take advantage of emittance damping, the region of possible machine operation in the particle energy / machine size parameter-space was defined. The maximum luminosities that are possible in the possible region were calculated. The main conclusions resulting from this study are:

- For a IR debris power limit of 50 kW/beam, the maximum proton energy achievable is ~100 TeV.
- Assuming that a synchrotron radiation peak power of 10 W/m/beam can be tolerated, the synchrotron radiation power becomes a softer limit, than e.g. magnet technology (here assumed to be limited to 15 T) or IR-debris power.
- The choice of a maximum of 60 events per crossing at a bunch spacing time of 12 ns, is a softer limit than the IR-debris power limitation.
- Luminosities of the order of $10^{35}cm^{-2}s^{-1}$ can only be achieved at lower particle energies. This is related not only to the IR and SR power limitations but also to the total machine power limitation (not discussed in detail here) that is roughly correlated with beam energy and luminosity through LE~P [2].
- The line of maximum luminosity goes from very high fields (15 T) at lower energy (40 TeV per beam) to high fields (9 T) at 70 TeV per beam, to moderate fields (8-9 T) at 100 TeV per beam. The maximum luminosities achievable are of the order of 10^{35} $cm^{-2}sec^{-1}$.
- The stored beam energy limitation limits the luminosity in machines that are larger than the currently proposed VLHC.

- The most serious beam-stability limitations after beam-beam tune-shift are of the transverse type, i.e. the resistive wall instability and TMCI. “Low” energy machines of large size are more likely to be affected by this problem. However, beam stability is considered a “soft” limitation because there are many coping mechanisms at hand. Beam-stability is a major issue regarding the minimum required magnet aperture and thus an important cost driver.

It has to be noted that these conclusions have been derived from a specific set of limitations and fixed parameters and will therefore change if one of these parameters is modified. As the most important result of this study appears the need for further investigation of the issue of IR debris power, since this is the parameter which was found to be the most limiting of all.

6.0 REFERENCES

[1] P. Bauer, “*Synchrotron Radiation Issues in Future Large Hadron Colliders*”, Fermilab Technical Division Note TD-01-061, July 2001;
[2] S. Peggs et al., “*VLHC Accelerator Physics*”, BNL, C-AD/AP/49, June 2001;
[3] P. Limon et al., “*VLHC Feasibility Study 2001*”, Fermilab TM 2149 or at www.vlhc.org;
[4] C. Darve, “*VLHC beam-screen cooling*”, Fermilab, Technical Division Note TD-01-005, Feb. 2001;
[5] A. Chou, “*Summary of the VLHC beam stability workshop at SLAC, March 2001”*, SLAC PUB 8000, May 2001;

7.0 APPENDIX

7.1 Table 4

The following table lists the main parameters of the VLHC simulations. The peak SR-power was limited to 10 W/m/beam (which typically corresponds to an average power of 5 W/m/beam). The peak IR power to 50 kW/beam. The maximum number of events per crossing to 60. The luminosity vs. damping time ratio listed in the table refers to the peak luminosity and the initial bunch population. Typically the ratio peaks later in the store. Therefore, most cases in the table were allowed to go to a τ ratio as low as 1. As can be seen in the comment column in the table, some solutions could not be fit within these constraints. These solutions lie at the edges or outside the “allowed” region, as can be seen in Figure 4. Beam Stability limitations were not taken into account. The limiting parameter in each case in Table 4 is outlined in bold. The peak luminosities from this table are plotted in Figure 5.

Table 4: VLHC simulations for different particle energy and machine size combinations. Beam-Beam, SR power, IR power and number of events limits included.

E/p^+ TeV	ρ (km)	B (T)	L_{peak} $x10^{34}$ $cm^{-2}s^{-1}$	$L_{average}$ $x10^{34}$ $cm^{-2}s^{-1}$	I_{ini} (mA)	$P^{peak}{}_{SR}$ (W/m/ beam)	$P^{peak}{}_{IR}$ (kW/ beam)	$N^{peak}{}_{X}$	$?^{peak}$ $\cdot 10^{-3}$	$\tau_L/\tau_{rad}{}^{ini}$	comment

20	3	22	7.2	4.8	457	**10**	9.3	35	7	2.6	OK
20	10	6.7	2.68	2.43	216	0.43	3.45	13	6.6	0.97	OK
25	4	21	5.3	3.4	312	**10**	10	30	**8**	3	OK
25	6	14	9.6	6.4	409	5.5	18	**54**	**8**	1.4	OK
25	9	9.3	10	7.4	457	2.7	19	**56**	**8**	1	OK
30	5	20	4.8	2.95	252	**10.1**	12.3	31	5	3.2	OK
30	6.5	15	7.6	5.5	324	7.35	19.7	49	7.5	1.95	OK
30	7	14.3	4.2	2.7	180	3.7	11	27	**8**	1.9	OK
30	9	11.1	2	1.23	96	1.2	5.1	13	7	1.6	OK
30	10	10	9.5	6.6	360	3.6	24	**61**	8	1.2	OK
30	11	9.1	**1.1**	**0.7**	60	0.5	2.8	7	7	1.5	NO
30	13	7.7	**1.7**	**1**	84	0.5	4.3	11	**8**	1.2	NO
30	20	5	**1**	**0.5**	53.5	0.3	2.6	6.4	2.3	1.84	NO
35	6	19.5	3.6	2.14	186	**9.6**	12	26	4.5	2.1	OK
35	8	14.6	8.8	5.3	276	8	30	**64**	**8**	1.7	OK
35	10	11.7	7.5	4.7	240	4.5	25	**54**	8	1.4	OK
40	7	19	3.2	1.9	156	**10.1**	13.7	26	**8**	4.1	OK
40	9	14.9	7.9	4.5	228	9	34	**63**	**8**	1.9	OK
40	10	13	7.6	4.5	216	6.8	33	**61**	**8**	1.65	OK
40	11	12.1	2.6	1.6	96	2.5	11.1	21	**7**	2	OK
40	13	10	7.4	4.7	216	4.1	32	**59**	**8**	1.3	OK
40	15	8.9	2.5	1.43	84	1.2	10.7	20	**8**	1.3	**?**
40	16	8	7.4	4.8	228	2.8	31	**59**	**8**	1.1	OK
40	19	7	4.2	2.6	144	1.3	18	34	**8**	1.1	OK
40	20	6.7	2.3	1.33	84	0.7	10.4	18	**8**	1	OK
40	25	5.3	**1.9**	**1.65**	84	0.4	8.1	15	**8**	**1**	NO
45	10	15	7.6	4.4	204	**10.4**	40	**67**	**8**	2	OK
45	12	12.5	7.5	4.4	192	6.8	40	**66**	**8**	1.6	OK
45	15	10	6.9	4.2	180	4	37	**61**	**8**	1.3	OK
45	20	7.5	5.8	3.7	168	2.1	31	51	**8**	**1**	OK
45	25	6	4	2.5	132	1	21	35	**8**	**1**	OK
45	30	5	3	2.4	120	0.7	16	26	**8**	**1**	OK
45	35	4.3	**2**	**1.8**	96	0.4	11	18	**8**	**1**	OK
50	7	24	**0.4**	**0.28**	60	**9.4**	3	3.8	1	2.0	NO
50	9	18.5	2.2	1.3	108	**10.3**	14.1	21	3	5.2	OK
50	10	17	3.75	2.2	132	**10.2**	24	36	5	3.3	OK
50	12	14	6	3.4	156	8.4	38	**58**	7.6	2.05	OK
50	13	13	6.4	3.6	156	7.14	41	**61**	7.9	1.8	OK
50	15	11.1	4.8	2.83	120	4.1	31	46	**8**	1.5	OK
50	16	10	6.6	3.8	156	4.7	42	**63**	**8**	1.4	OK
50	16.5	10	6.5	6	228	6.5	42	**62**	6	2	OK
50	19	8.8	6.4	3.8	156	3.3	41	**61**	**8**	1.2	OK
50	20	8.3	4.2	2.4	108	2.1	27	40	**8**	1.2	OK
50	25	6.7	2.9	2.9	84	1	19	28	**8**	**1.1**	OK
50	30	5.6	**1.8**	**1**	60	0.5	12	17	**8**	**1**	NO
55	13	14.1	6.6	3.8	156	**10.5**	**51**	**69**	7.5	2.1	OK
55	15	12.2	6.6	3.6	144	7.3	**51**	**69**	**8**	1.7	OK
55	17	10.8	6	3.4	132	5.2	46	**63**	**8**	1.5	OK
55	20	9.2	4.7	2.7	108	3.1	36	49	**8**	1.3	OK
55	24	7.6	3.4	1.94	84	1.7	26	36	**8**	1.2	OK
55	29	6.3	2.6	1.5	72	1	20	27	**8**	**1.1**	OK
60	10	20	**1.1**	**0.65**	72	**11.6**	10	12.3	2	9.2	NO
60	12	16.7	2.4	1.4	90	**10**	22	27	4	4.4	OK

60	13	15.4	3.7	2.1	108	**10.3**	33	41.3	5	3.2	OK
60	15	13.3	5.2	2.9	120	8.6	**47**	**58**	7	2.2	OK
60	16	12.5	5.5	2.97	120	7.5	**49**	**61**	7.7	2	OK
60	17	12	4.9	2.7	108	6	44	55	**8**	1.8	OK
60	18	11	5.05	2.84	108	5.3	45	56	**8**	1.7	OK
60	19	10.5	5.16	2.9	108	4.8	46	**57.8**	**8**	1.5	OK
60	20	10	5.2	2.9	108	4.3	46.6	58	**8**	1.5	OK
60	22	9	5.2	2.9	108	3.6	47	**58**	**8**	1.3	OK
60	25	8	3.8	2.1	84	2.2	34	43	**8**	1.2	OK
60	30	6.7	2.4	1.4	60	1	32	27	**8**	1.2	OK
65	15	14.5	4	2.5	102	**10**	42	48	5.4	2.8	OK
65	17	12.8	4.8	2.8	106	8	**50**	58	7	2.2	OK
65	20	10.8	5	2.8	100	5.5	**52**	**60**	**8**	1.7	OK
65	25	8.7	4.9	2.9	96	3.4	**51**	**59**	**8**	1.3	OK
65	29	7.5	4	2.3	84	2.2	42	48	**8**	1.2	OK
65	31	7	3.8	2.2	82	1.9	40	46	**8**	1.2	OK
70	13	17.9	**1.2**	**0.7**	60	**10.5**	14	15	2.2	7.6	NO
70	15	15.6	2.2	1.23	72	**9.5**	26.3	28	3.6	4.3	OK
70	15.5	15	2.1	1.7	84	**10.4**	25	27	2.5	5	OK
70	17	13.4	4.2	2.3	96	**9.9**	**50**	54	6	2.6	OK
70	19	12.3	4.3	2.3	90	7.4	**51.5**	**55**	7	2.2	OK
70	21	11.1	4.2	2.2	84	5.7	**50**	54	7	1.9	OK
70	23.5	10	4.2	3.3	107	7.4	**50**	54	4.2	2.7	OK
70	25	9.3	3.7	2.1	72	3.4	44	47	**8**	1.5	OK
70	30	7.8	3	1.6	60	3	36	38	**8**	1.3	OK
70	35	6.7	2.2	1.2	48	1.2	26	28	**8**	1.2	OK
75	17	14.7	2.6	1.4	72	**9.8**	35	35	4	3.7	OK
75	19	13.2	3.8	2.1	84	9.1	**52**	52	6	2.6	OK
75	23	10.9	3.7	1.9	72	5.3	**50**	50	7	2.5	OK
75	26	9.6	3.5	1.95	66	3.8	**48**	47	**8**	1.6	OK
75	30	8.4	3.4	1.9	64	2.8	46	46	**8**	1.4	OK
75	33	7.6	3.4	1.85	64	2.3	46	46	**8**	1.3	OK
80	15	17.8	**1**	**0.54**	48	**10.8**	34	32	2	3.8	NO
80	16	16.7	**1.58**	**0.9**	60	**11.9**	24	22.7	2.6	6.15	NO
80	17	15.7	**1.8**	**1**	60	**10.5**	28	26	3	5	NO
80	19	14	3	1.64	72	**10.1**	46	43	4	3.3	OK
80	21	12.7	3.4	1.85	72	8.3	**52**	49	5.4	2.6	OK
80	23	11.6	3.3	1.72	66	6.3	**51**	48	6	2.3	OK
80	25	10.7	3	1.6	60	5	46	43	**8**	2.1	OK
80	30	8.9	2.5	1.39	48	2.7	38.5	36	**8**	1.7	OK
80	35	7.6	**2**	**0.97**	36	1.5	31	29	**8**	1.3	OK
85	20	14.2	2.3	1.27	60	**10**	40	35	4	3.8	OK
85	22	12.9	3	1.7	66	8.8	**52**	45	5	2.9	OK
85	24	11.8	3	1.64	61	6.9	**52**	46	5	2.5	OK
85	26	10.9	3	1.54	58	5.5	**52**	46	6	2.2	OK
85	28	10.1	3	1.58	55	4.6	**52**	46	6.5	1.94	OK
85	30	9.5	3	1.6	54	3.9	**52**	46	7	1.8	OK
90	19	15.8	**1.34**	**0.77**	48	**10.8**	26	21	2.5	6.3	NO
90	20	15	**1**	**0.84**	48	**10**	20	16	1.7	8	NO
90	21	14.3	2	1.12	54	**10**	39	32	3.4	4.3	OK
90	23	13.1	2.9	1.61	62	9.6	**56**	46	4.6	3.1	OK
90	25	12	2.7	1.46	55	7.2	**52**	43	5	2.7	OK
90	27	11.1	2.6	1.33	50	5.6	**50**	42	5.3	2.4	OK

95	22	14.4	**1.7**	**0.95**	48	**10**	36.2	29	3	4.8	NO
95	24	13.2	2.6	1.4	56	**9.9**	**55**	44	4.2	3.4	OK
95	26	12.2	2.83	1.22	48	7.2	**48**	38	4.3	3.1	OK
100	23	14.5	**1.6**	**0.87**	44	**10.4**	37.5	28	3	5	NO
100	25	13.3	2	1.13	48	**9.5**	47	35	3.6	3.9	OK
100	27	12.3	2.3	1.27	48	8.2	**54**	41	4.3	3.2	OK
100	29	11.5	2.3	1.21	44	6.5	**54**	41	5	2.8	OK
110	24.5	15	**0.88**	**0.6**	32	**9.8**	16.4	11	2	11.5	NO
110	36.5	10	2.71	2	66	9	**56**	38	1.2	4.6	OK
110	74	5	2.8	2	72	2.4	**51**	35	2	2.7	OK

7.2 Table 5

The limiting parameter in the simulations tabulated in the following, is SR- power and beam-beam tune-shift only. The IR-power limitation was removed in this case. The limiting parameter in each case in the table is outlined in bold. The luminosities in the table are plotted in Figure 6.

Table 5: VLHC simulations for different particle energy and machine size combinations. Beam-beam and SR power limits only.

E/p^+ TeV	ρ (km)	B (T)	L_{peak} $x10^{34}$ $cm^{-2}s^{-1}$	$L_{average}$ $x10^{34}$ $cm^{-2}s^{-1}$	I_{ini} (mA)	P^{peak}_{SR} (W/m/ beam)	P^{peak}_{IR} (kW/ beam)	N^{peak}_{X}	$?^{peak}$ $\cdot 10^{-3}$	τ_L/τ_{rad}^{ini}	comment
25	4	21	5.3	3.4	312	**10**	10	30	**8**	3	OK
25	6	14	19.3	13.2	745	**10**	36	108	**8**	1.3	OK
25	9	9.3	35	25	1189	7	66	197	**8**	0.8	OK
30	5	20	4.8	2.95	252	**10.1**	12.3	31	5	3.2	OK
30	6.5	15	12.3	7.6	427	**10**	32	79	**8**	1.6	OK
30	7	14.3	14.5	9.2	493	**10**	37	93	**8**	1.5	OK
30	9	11.1	25	18	811	**10**	65	161	**8**	1.1	OK
30	11	9.1	41	33	1183	**10**	106	263	**8**	0.8	OK
30	13	7.7	41	33	1183	7	106	263	**8**	**0.7**	NO
30	20	5	41	33	1183	2.9	90	225	**8**	**0.5**	NO
35	6	19.5	3.8	2.24	192	**10**	12.8	28	**8**	3.7	OK
35	8	14.6	11.4	6.7	341	**10**	39	82	**8**	1.6	OK
35	10	11.7	18.4	12.4	541	**10**	62	133	**8**	1.3	OK
40	7	19	3.2	1.9	156	**10.1**	13.7	26	**8**	4.1	OK
40	9	14.9	9.3	5.3	258	**10**	40	75	**8**	1.8	OK
40	11	12.1	14.5	9	384	**10**	62	116	**8**	1.4	OK
40	15	8.9	27.7	21	709	**10**	119	222	**8**	1	OK
40	20	6.7	55	43	1183	**10**	236	441	**8**	**0.5**	NO
40	25	5.3	55	43	1183	6	236	441	**8**	**0.5**	NO
45	10	15	7.6	4.4	204	**10.4**	40	67	**8**	2	OK
45	12	12.5	11.8	6.9	285	**10**	63	104	**8**	1.5	OK
45	15	10	18.7	12.4	445	**10**	99	165	**8**	1.2	OK
45	20	7.5	34.9	27.1	793	**10**	185	308	**8**	0.9	OK
45	25	6	62	49	1183	**10**	329	547	**8**	**0.4**	NO
45	30	5	62	49	1183	6.7	329	547	**8**	**0.4**	NO
45	35	4.3	62	49	1183	4.9	329	547	**8**	**0.4**	NO
50	9	18.5	2.2	1.3	108	**10.3**	14.1	21	3	5.2	OK
50	15	11.1	13.2	7.8	288	**10**	85	127	**8**	1.4	OK
50	16.5	10	16.3	10.2	354	**10**	104	156	**8**	1.3	OK
50	20	8.3	24	17	523	**10.1**	154	231	**8**	1	OK

50	25	6.7	38.6	30.8	805	**10**	248	371	**8**	**0.8**	OK
50	30	5.6	66.5	50.3	1165	**10**	427	639	**8**	**0.6**	NO
55	13	14.1	6.6	3.8	156	**10.5**	51	69	7.5	2.1	OK
55	15	12.2	9.7	5.4	198	**10**	75	101	**8**	1.6	OK
55	17	10.8	13.2	7.7	264	**10.4**	101	138	**8**	1.4	OK
55	20	9.2	17.9	11.4	360	**10.2**	137	187	**8**	1.2	OK
55	24	7.6	25.12	18	511	**10**	192	262	**8**	1	OK
55	29	6.3	37.9	30.4	745	**10**	290	395	**8**	**0.8**	OK
60	12	16.7	2.4	1.4	90	**10**	22	27	4	4.4	OK
60	15	13.3	6.5	3.7	141	**10**	58	73	**8**	2	OK
60	17	12	9.6	5.3	181	**10**	87	108	**8**	1.6	OK
60	20	10	13.4	7.8	250	**10**	120	150	**8**	1.3	OK
60	25	8	20.6	13.6	390	**10**	185	231	**8**	1.1	OK
60	30	6.7	29.7	22.3	565	**10**	267	333	**8**	0.9	OK
65	15	14.5	4	2.5	102	**10**	42	48	5.4	2.8	OK
65	17	12.8	6.6	3.8	132	**10**	69	79	**8**	2	OK
65	20	10.8	10.5	5.7	183	**10**	109	126	**8**	1.5	OK
65	25	8.7	16.1	9.7	284	**10**	168	193	**8**	1.2	OK
65	29	7.5	21.5	14.3	384	**10**	224	259	**8**	1	OK
65	31	7	24.2	16.8	436	**10**	252	291	**8**	1	OK
65	35	6.2	30.5	23	553	**10**	318	367	**8**	0.9	OK
65	40	5.4	41.3	34.2	726	**10**	431	496	**8**	**0.7**	NO
70	15	15.6	2.2	1.23	72	**9.5**	26.3	28	3.6	4.3	OK
70	15.5	15	2.1	1.7	84	**10.4**	25	27	2.5	5	OK
70	17	13.4	4.2	2.3	96	**9.9**	**50**	54	6	2.6	OK
70	19	12.3	6.7	3.7	123	**10**	80	86	**8**	1.9	OK
70	21	11.1	8.9	4.8	148	**10**	107	114	**8**	1.5	OK
70	23.5	10	11.4	6.3	186	**10**	137	146	**8**	1.4	OK
70	25	9.3	12.9	7.3	211	**10**	155	165	**8**	1.3	OK
70	30	7.8	17.9	11.1	300	**10**	214	230	**8**	1.1	OK
70	35	6.7	24.2	16.7	415	**10**	290	310	**8**	1	OK
70	40	5.8	32	24	541	**10**	383	410	**8**	0.8	OK
70	45	5.2	40.4	33.5	685	**10**	484	518	**8**	**0.7**	NO
70	50	4.7	52.5	46.2	847	**10**	509	545	**8**	**0.8**	NO
75	17	14.7	2.6	1.4	72	**9.8**	35	35	4	3.7	OK
75	19	13.2	4.5	2.5	93	**10**	61	61	**8**	2.4	OK
75	23	10.9	8.7	4.6	136	**10**	119	119	**8**	1.5	OK
75	26	9.6	11.3	6.2	174	**10**	154	154	**8**	1.3	OK
75	30	8.4	14.9	8.6	232	**10**	203	203	**8**	1.2	OK
75	33	7.6	17.6	10.8	279	**10**	240	240	**8**	1.1	OK
75	40	6.2	25	17.1	409	**10**	341	341	**8**	0.9	OK
75	45	5.6	32	24	523	**10**	436	436	**8**	0.82	OK
75	50	5	39	32.3	643	**10**	532	531	**8**	0.7	OK
80	15	17.8	**1**	**0.54**	48	**10.8**	34	32	2	3.8	NO
80	17	15.7	**1.8**	**1**	60	**10.5**	28	26	3	5	NO
80	19	14	3	1.64	72	**10.1**	46	43	4	3.3	OK
80	21	12.7	4.57	2.5	88	**10.1**	70	66	6.2	2.4	OK
80	23	11.6	6.4	3.5	105	**10**	99	93	**8**	1.8	OK
80	25	10.7	8.3	4.4	124	**10**	128	120	**8**	1.5	OK
80	30	8.9	12.1	6.7	178	**10**	186	174	**8**	1.3	OK
80	35	7.6	16.2	9.6	243	**10**	249	234	**8**	1.1	OK
80	40	6.7	20.7	13.5	318	**10**	319	298	**8**	1	OK
80	45	5.9	25.6	18.2	403	**10**	394	369	**8**	0.9	OK

85	20	14.2	2.3	1.27	60	**10**	40	35	4	3.8	OK
85	22	12.9	3.8	2.1	76	**10**	66	58	5.5	2.7	OK
85	24	11.8	5.4	3	90	**10**	93	82	7	2	OK
85	26	10.9	7.2	3.8	106	**10**	124	110	**8**	1.7	OK
85	28	10.1	8.8	4.6	123	**10**	152	134	**8**	1.5	OK
85	30	9.5	10.1	5.4	141	**10**	174	154	**8**	1.4	OK
85	35	8.1	13.6	7.6	191	**10**	235	207	**8**	1.2	OK
85	40	7.1	17.4	10.6	250	**10**	300	265	**8**	1	OK
85	45	6.3	21.2	14.1	315	**10**	366	323	**8**	1	OK
85	50	5.7	25.7	18.5	390	**10**	443	391	**8**	0.9	OK
90	19	15.8	**1.34**	**0.77**	48	**10.8**	26	21	2.5	6.3	NO
90	20	15	**1**	**0.84**	48	**10**	20	16	1.7	8	NO
90	21	14.3	2	1.12	54	**10**	39	32	3.4	4.3	OK
90	23	13.1	3.2	1.74	65	**10**	62	51	4.8	3	OK
90	25	12	4.6	2.5	77	**10**	88	74	6.2	2.2	OK
90	27	11.1	6.1	3.3	90	**10**	117	98	7.7	1.8	OK
90	30	10	8.4	4.3	112	**10**	162	135	**8**	1.5	OK
90	35	8.6	11.5	6.1	151	**10**	221	184	**8**	1.3	OK
90	40	7.5	14.6	8.3	198	**10**	281	234	**8**	1.1	OK
90	45	6.7	17.9	11.1	250	**10**	344	287	**8**	1	OK
90	50	6	21.6	14.6	310	**10**	415	346	**8**	1	OK
95	22	14.4	**1.7**	**0.95**	48	**10**	36.2	29	3	4.8	NO
95	24	13.2	2.6	1.4	56	**9.9**	**55**	44	4.2	3.4	OK
95	26	12.2	3.8	2	67	**10**	81	64	5.5	2.5	OK
95	30	10.6	6.6	3.5	90	**10**	141	111	**8**	1.7	OK
95	35	9	9.7	5	123	**10**	207	163	**8**	1.34	OK
95	40	7.9	12.5	6.7	160	**10**	266	210	**8**	1.2	OK
95	45	7	15.4	9	202	**10**	328	259	**8**	1	OK
95	50	6.3	18.4	11.6	249	**10**	392	309	**8**	1	OK
100	23	14.5	**1.6**	**0.87**	44	**10.4**	37.5	28	3	5	NO
100	25	13.3	2.2	1.2	51	**10**	52	39	3.8	3.8	OK
100	27	12.3	3.3	1.8	59	**10**	78	58	5	2.8	OK
100	29	11.5	4.4	2.4	68	**10**	104	78	6.2	2.2	OK
100	35	9.5	8.2	4.2	100	**10**	193	145	**8**	1.4	OK
100	40	8.3	10.7	5.6	130	**10**	252	188	**8**	1.3	OK
100	45	7.4	13.3	7.3	165	**10**	312	234	**8**	1.1	OK
100	50	6.7	16	9.5	203	**10**	376	282	**8**	1	OK
110	24.5	15	**0.88**	**0.6**	32	**9.8**	16.4	11	2	11.5	NO
110	36.5	10	6	3.2	74	**10**	169	116	**8**	1.7	OK
110	45	8.1	10	5.1	112	**10**	282	192	**8**	1.3	OK
110	74	5	**1.8**	**2.8**	72	2.4	**51**	35	2	2.7	NO

7.3 Table 6

The limiting parameter in the simulations tabulated in Table 6 were: SR- power, beam-beam tune-shift and the beam stability parameters (resistive wall, Laslett tune-shift, TMCI). No IR-power or number of events limit assumed. The limiting parameter in each case in the table is outlined in bold. The peak luminosities are plotted in Figure 7.

Table 6: VLHC simulations for different particle energy and machine size combinations. Beam-beam, beam stability (TMCI, resistive wall and coherent Laslett tune-shift) and SR power limits only.

E/p^+ TeV	ρ (km)	B (T)	L_{peak} $\cdot 10^{34}$ $cm^{-2}s^{-1}$	$L_{average}$ $\cdot 10^{34}$ $cm^{-2}s^{-1}$	N_{ini} $\cdot 10^{10}$	I_{ini} (mA)	P^{peak}_{SR} (W/m/ beam)	P^{peak}_{IR} (kW/ beam)	N^{peak}_{X}	$?^{peak}$ $\cdot 10^{-3}$	N_{TMCI} $\cdot 10^{10}$	τ_{RW} turns	δQ_L	τ_L/τ_{rad}^{in}
30	5	20	4.7	2.9	2.08	250	**10**	12	31	5.4	3.3	6.7	0.14	3.3
30	7	14.3	7.8	4.9	2.4	288	5.9	20	50	**8**	2.48	3.3	**0.21**	1.6
30	9	11.1	6.2	4	2	240	3	16	40	**8**	**2**	2.5	**0.2**	1.3
30	11	9.1	4.9	3.1	1.68	202	1.7	16	40	**8**	**1.7**	1.9	**0.2**	1.1
30	13	7.7	3.9	2.5	1.443	173	1	10	25	**8**	**1.4**	1.8	**0.2**	1
30	15	6.7	3.1	2	1.267	152	0.7	8	20	**8**	**1.267**	1.6	**0.2**	1
40	7	19	3.2	1.9	1.3	156	**10**	14	26	4.2	3.3	7.9	0.09	4
40	9	14.9	9.3	5.3	2.15	258	**10**	40	75	**8**	2.67	3.2	0.17	1.8
40	11	12.1	9.8	5.9	2.237	269	7	42	79	**8**	**2.24**	2.3	**0.2**	1.5
40	15	8.9	6.7	4.2	1.69	203	2.9	29	54	**8**	**1.69**	1.7	**0.2**	1.2
40	20	6.7	4.4	2.8	1.293	155	1.23	19	36	**8**	**1.293**	1.2	**0.2**	1
40	25	5.3	3	2.5	1.048	126	0.64	13	25	7.7	**1.048**	**1**	**0.2**	1
50	9	18.5	2.2	1.3	0.88	106	**10**	14	21	3.2	3.4	9.2	0.06	5
50	13	12.8	9.8	5.5	1.82	219	**10**	63	95	**8**	2.4	2.4	0.15	1.6
50	15	11.1	11.4	6.6	2.1	252	8.9	73	110	**8**	**2.1**	1.8	**0.2**	1.4
50	20	8.3	7.9	4.9	1.616	194	3.8	51	76	**8**	**1.616**	1.3	**0.2**	1.2
50	25	6.7	5.7	3.6	1.309	157	1.95	37	55	**8**	**1.309**	1	**0.2**	1
50	30	5.6	3.4	2.1	0.9	108	0.9	22	33	**8**	1.1	**0.95**	0.16	1
60	12	16.7	2.4	1.4	0.75	90	**10**	22	27	3.7	3.1	7.3	0.05	4.4
60	15	13.3	6.6	3.7	1.18	142	**10**	60	74	7.7	2.5	3	0.09	2
60	17	12	9.5	5.2	1.5	180	**10**	86	107	**8**	2.3	2	0.13	1.6
60	20	10	12.8	7.4	2	240	9.6	115	144	**8**	**1.9**	1.3	**0.2**	1.3
60	25	8	8.8	5.4	1.5	180	4.6	79	99	**8**	**1.6**	1.1	0.19	1.1
60	30	6.7	5.2	3.2	1	120	2.14	47	59	**8**	1.3	**1**	0.15	1
70	15	15.6	2.4	1.4	0.635	76	**10**	29	31	3.7	2.96	6.4	0.04	4.1
70	17	13.4	4.3	2.4	0.81	97	**10**	58	55	5.7	2.6	3.8	0.06	2.6
70	19	12.3	6.7	3.7	1.02	123	**10**	80	86	**8**	2.4	2.5	0.09	1.9
70	21	11.1	9	4.8	1.24	149	**10**	108	116	**8**	2.2	1.8	0.11	1.5
70	23.5	10	11.4	6.3	1.55	186	**10**	137	146	**8**	1.9	1.3	0.16	1.4
70	25	9.3	13	7.3	1.76	211	**10**	156	167	**8**	1.8	1.1	0.19	1.3
70	27	8.6	12.6	7.3	1.76	211	8.6	151	162	**8**	**1.7**	**1**	**0.2**	1.2
70	30	7.8	10.3	6.2	1.5	180	6	123	132	**8**	1.54	**0.9**	0.19	1.1
70	35	6.7	4.9	2.8	0.8	96	2.3	59	63	**8**	1.3	**0.98**	0.12	1.1
70	40	5.8	2.7	1.5	0.5	60	1.1	33	35	**8**	1.2	**1**	0.08	1.1
70	45	5.2	1.9	1	0.4	48	0.7	23	25	**8**	1	**0.99**	0.07	1
80	15	17.8	**0.8**	**0.5**	0.37	44	**10**	13	12	1.7	3.4	13.5	0.02	9.6
80	17	15.7	**0.9**	**0.6**	0.475	57	**10**	14	13	2.9	3	10.3	0.03	9.6
80	19	14	2.9	1.6	0.595	71	**10**	45	42	4.4	2.7	4.7	0.04	3.4
80	21	12.7	4.6	2.5	0.73	88	**10**	71	67	6.2	2.5	3.2	0.06	2.4
80	23	11.6	6.4	3.5	0.87	105	**10**	99	93	**8**	2.3	2.3	0.08	1.8
80	25	10.7	8.3	4.4	1.03	124	**10**	128	120	**8**	2.1	1.7	0.1	1.5
80	28	9.5	10.7	5.8	1.3	156	**10**	165	155	**8**	1.9	1.2	0.13	1.35
80	30	8.9	12.3	6.7	1.49	179	**10**	189.2	178	**8**	1.76	1	0.16	1.26
80	32	8.4	12.1	6.8	1.5	180	8.9	187	175	**8**	1.66	**0.9**	0.17	1.2
80	35	7.6	7.6	4.3	1	120	5	117	110	**8**	1.5	**0.96**	0.13	1.2
80	40	6.7	5.2	2.9	0.75	90	2.9	80	75	**8**	1.3	**0.9**	0.11	1.1
80	50	5.3	2	1	0.35	42	0.8	31	29	**8**	1.1	**0.96**	0.06	1.1
85	20	14.2	2.4	1.4	0.52	62	**10**	42	37	4	2.8	5.2	0.04	3.8

85	22	12.9	3.8	2.1	0.63	76	**10**	65.6	58	5.4	2.5	3.5	0.05	2.7
85	24	11.8	5.5	3	0.75	90	**10**	95	84	7	2.3	2.5	0.06	2
85	26	10.9	7.2	3.8	0.88	106	**10**	124	110	**8**	2.2	1.9	0.08	1.7
85	28	10.1	8.8	4.6	1.02	123	**10**	152	134	**8**	2	1.5	0.1	1.5
85	30	9.5	10.1	5.4	1.17	141	**10**	174	154	**8**	1.9	1.2	0.12	1.4
85	35	8.1	10.6	5.5	1.2	144	7.6	173	152	**8**	1.6	**0.92**	0.14	1.2
85	40	7.1	6.2	3.4	0.8	96	3.9	107	95	**8**	1.4	**0.91**	0.11	1.1
85	50	5.7	2.7	1.5	0.42	50	1.3	47	41	**8**	1.1	**0.91**	0.07	1
90	19	15.8	**1.2**	**0.7**	0.371	45	**10**	23.1	20	2.3	3.1	8.7	0.02	6.5
90	20	15	**1.6**	**0.9**	0.414	50	**10**	30.8	26	2.8	2.9	6.9	0.03	5
90	21	14.3	2	1.1	0.455	55	**10**	39	32	3.5	2.8	5.7	0.03	4.3
90	23	13.1	3.2	1.7	0.545	65	**10**	62	52	4.8	2.6	3.8	0.04	3
90	25	12	4.5	2.5	0.645	77	**10**	87	72	6.3	2.4	2.8	0.05	2.3
90	27	11.1	6.1	3.3	0.75	90	**10**	117	98	7.7	2.2	2.1	0.07	1.8
90	30	10	8.4	4.3	0.93	112	**10**	162	135	**8**	1.98	1.5	0.09	1.5
90	32	9.4	9.7	5	1.06	127	**10**	187	156	**8**	1.86	1.2	0.11	1.4
90	35	8.6	10.8	5.7	1.2	144	9.6	208	173	**8**	1.71	**0.97**	0.14	1.3
90	40	7.5	6.7	3.8	0.8	96	4.9	129	108	**8**	1.5	**0.96**	0.1	1.2
90	45	6.7	3.8	2	0.5	60	2.4	73	61	**8**	1.34	**1**	0.07	1.2
90	50	6	2.5	1.3	0.36	43	1.4	48.1	40	**8**	1.2	**1**	0.06	1.15
100	23	14.5	**1.6**	**0.87**	0.357	44	**10.4**	37.5	28	3	2.8	6.5	0.03	5
100	25	13.3	2.2	1.2	0.422	51	**10**	52	39	3.8	2.6	4.6	0.03	3.8
100	27	12.3	3.3	1.8	0.495	59	**10**	78	58	5	2.4	3.3	0.04	2.8
100	29	11.5	4.4	2.4	0.57	68	**10**	104	75	6	2.3	2.5	0.03	2.2
100	35	9.5	8.2	4.2	0.83	100	**10**	193	145	**8**	1.9	1.3	0.08	1.4
100	37	9	9.2	4.8	0.93	112	**10**	217	162	**8**	1.8	1.1	0.1	1.4
100	40	8.3	9.1	4.6	0.93	112	8.6	214	161	**8**	1.7	**0.96**	0.11	1.3
100	45	7.4	5.4	2.9	0.6	72	4.4	127	95	**8**	1.5	**1**	0.08	1.2
100	50	6.7	3.2	1.7	0.4	48	2.4	76	57	**8**	1.34	**1**	0.06	1.2
110	28	13.1	2	1.1	0.363	44	**10**	57	39	3.5	2.6	4.6	0.03	3.9
110	30	12.2	2.8	1.5	0.415	50	**10**	79	54	4.5	2.4	3.4	0.03	3
110	35	10.5	5.2	2.8	0.565	68	**10**	147	100	7.1	2.1	1.9	0.05	1.9
110	37	9.9	6.3	3.3	0.635	76	**10**	178	121	**8**	2	1.5	0.06	1.7
110	40	9.2	7.9	4	0.74	89	**10**	223	152	**8**	1.8	1.2	0.08	1.4
110	42	8.7	8.7	4.4	0.81	97	**10**	246	167	**8**	1.751	1	0.09	1.3
110	45	8.2	8	3.9	0.76	91	8.2	226	154	**8**	1.64	**0.95**	0.09	1.3
110	50	7.3	4.8	2.5	0.5	60	4.4	135	92	**8**	1.5	**1**	0.06	1.3